Die approbierte Originalversion dieser Diplom-/Masterarbeit ist in der Hauptbibliothek der Technischen Universität Wien aufgestellt und zugänglich.
http://www.ub.tuwien.ac.at

The approved original version of this diploma or master thesis is available at the main library of the Vienna University of Technology.
http://www.ub.tuwien.ac.at/eng

TECHNISCHE UNIVERSITÄT WIEN
Vienna University of Technology

INSTITUT FÜR MECHANIK UND MECHATRONIK
Mechanics & Mechatronics

DIPLOMARBEIT

Global predictive control for smart homes using improved disturbance predictions

ausgeführt zum Zwecke der Erlangung des akademischen Grades eines Diplom-Ingenieurs
unter der Leitung von

Ao.Univ.Prof. Dr. Martin Kozek und
DI Dr. techn. Michaela Killian
Institut für Mechanik und Mechatronik
Abteilung für Regelungstechnik und Prozessautomatisierung

eingereicht an der Technischen Universität Wien

Fakultät für Maschinenwesen und Betriebswissenschaften

von

Zauner Michael
Matr.Nr.: 01125895
Karl Gleichweitstr. 3
2500 Baden

Wien, am 8. Februar 2018

Zauner Michael

Eidesstattliche Erklärung

Ich erkläre eidesstattlich, dass ich die Arbeit selbständig angefertigt, keine anderen als die angegebenen Hilfsmittel benutzt und alle aus ungedruckten Quellen, gedruckter Literatur oder aus dem Internet im Wortlaut oder im wesentlichen Inhalt übernommenen Formulierungen und Konzepte gemäß den Richtlinien wissenschaftlicher Arbeiten zitiert, durch Fußnoten gekennzeichnet bzw. mit genauer Quellenangabe kenntlich gemacht habe.

Wien, am 8. Februar 2018 Zauner Michael

Danksagung

An dieser Stelle möchte ich mich bei all denjenigen bedanken, die mich während meines Studiums und bei der Anfertigung meiner Masterarbeit unterstützt haben.

Zuerst gebührt mein Dank Herrn Ao.Univ.Prof. Dipl.-Ing. Dr.techn. Kozek Martin und Frau Dipl.-Ing. Dr.techn. Killian Michaela, welche meine Masterarbeit betreut und begutachtet haben. Für die hervorragende Betreuung, den vielen fachlichen Inputs und der konstruktiven Kritik möchte ich mich an dieser Stelle herzlich bedanken.
Ebenfalls gebührt mein Dank der Firma evonHOME für die Bereitstellung des Projektes und der zur Verfügung gestellten Messdaten.

Einen besonderen Dank gilt ebenfalls all meinen Mitstudenten, die mit mir dieses Studium, auch wenn es nur teilweise war, bestritten haben. Ich möchte an dieser Stelle speziell meinen Freunden und Mitstudenten Erdogan Dennis, Müllner Stefan und Kadan Arnold danken.

Abschließend möchte ich mich ebenfalls bei meinen Eltern bedanken, die mir dieses Studium durch ihre Unterstützung ermöglicht haben.

Zauner Michael

Kurzfassung

Die Idee zur Verwendung von model predictive control (MPC) Algorithmen zur Regelung der thermischen Systeme eines smart-Home wird immer beliebter in modernen smart Homes. Die Effizienz und Performance von MPC Algorithmen hängt stark von der Güte der vorhandenen Störgrößenprädiktionen ab. Mit der Verbesserung der vorhandenen Wettervorhersage mittels Messdaten aus hausinternen Wetterstationen und selbstadaptierenden Belegschaftsprädiktionen könnte das smart-Home nicht nur besseren thermischen Komfort liefern, sondern auch noch elektrische Energie und Kosten sparen. Diese Arbeit stellt einen MPC Regler basierend auf gemischt-ganzzahliger quadratischen Optimierung vor. Der Regler integriert sowohl das thermische Model, als auch das elektrische Model, des smart-Home. Der Regelungsalgorithmus berechnet das globale Optimum unter Berücksichtigung möglicher Randbedingungen des smarten Stromnetzes. Deshalb kann der vorgestellte Regler die fortlaufenden monetären Stromkosten oder die verbrauchte Energie minimieren ohne dabei den thermischen Komfort zu verletzen. Ein weiteres Hauptmerkmal des Reglers ist, dass ein simples und intuitives Interface integriert wurde, welches den Bewohnern erlaubt den Regler auf ihre individuellen Wünsche anzupassen. Durchgeführte 'closed-loop' Simulationen zeigen die Effizienz der globalen Optimierung als auch alle weiteren Funktionen des vorgestellten Regelungskonzeptes.

Abstract

Model predictive control (MPC) schemes for managing thermal systems in a smart home are becoming more popular in modern smart homes. The efficiency and performance of MPC controllers greatly depends on the quality of the available predictions for the controller. By refining the available weather forecasts with measurements taken from localized weather stations integrated into the smart home and self-adaptive occupancy predictions, the smart home could not only provide better thermal comfort, but also save energy and reduce the costs for the residents. This thesis proposes a mixed-integer quadratic-programming model predictive control scheme based on the thermal smart home building model and the electrical system. The controller calculates the global optima with respect to possible smart grid load constraints. This enables the control scheme to minimize the consumed energy or operating costs of the smart home while also guaranteeing thermal comfort. Another key feature of the controller is the option to provide a simple and easy interface for the occupants of the smart home to tune their smart home in accordance to their individual preferences. Closed-loop simulation results showcase the efficient global optimization as well as all the features of the proposed controller.

Contents

1 Introduction **1**
1.1 Motivation . . . 1
1.2 Problem description . . . 2
1.3 Research questions . . . 3

2 Smart Home Model **4**
2.1 Thermal Model of the Smart Home . . . 5
2.2 Electrical Model of the Smart Home . . . 6
2.2.1 Overview . . . 6
2.2.2 Smart Home Appliances . . . 8
2.3 Heating System . . . 10

3 Weather Forecast **11**
3.1 Overview . . . 11
3.2 Ambient Temperature Forecast . . . 11
3.3 Solar Irradiation Forecast . . . 13

4 Occupancy Predictions **16**
4.1 Occupancy Comfort . . . 16
4.2 Occupancy Prediction . . . 18
4.2.1 Off-line Feature Extraction and Clustering . . . 18
4.2.2 On-line Occupancy Prediction . . . 19

5 Mixed-Integer Quadratic Programming MPC **21**
5.1 Overall Control Structure . . . 21
5.2 MIQP Cost Function . . . 22
5.3 User Weights . . . 24
5.4 Mixed-Integer Solver . . . 25

6 Results **26**
6.1 Overview . . . 26

6.2 Weather Forecast 26
6.2.1 Ambient Temperature Forecast 26
6.2.2 Solar Irradiation Forecast 28
6.3 MIQP-MPC 33
6.3.1 Performance Modes Comparison 34
6.3.2 Smart Grid Power Constraints 38
6.4 Parametric Study on MIQP-MPC Performance 40
6.4.1 Weather prediction impact 41
6.4.2 Occupcancy Prediction Impact 42

7 Discussion **44**

Bibliography **47**

Chapter 1

Introduction

1.1 Motivation

In the European Union about 40% of all energy is used for buildings. Heating and cooling amounts to 2/3 of the energy consumption in buildings. The biggest energy saving potential can be found in smaller buildings below 1000 m^2 as they are responsible for 80% of energy consumed in buildings [1].
By tackling the energy saving potential in residential buildings, which have been estimated to be about 27% - 30% [2], it is possible to decrease the future environmental impact and reduce the CO_2 emissions. With the growing degree of home automation and the increased spread of 'Internet of things' devices residential homes will become smarter. Today those so called smart homes usually integrate lighting control, access control and heating control. By using the already integrated sensors of a modern smart home and a more sophisticated occupancy prediction combined with smart algorithms, it is possible to reduce the operating costs as well as the energy demand of the smart home while offering the same level of user comfort.
Residential loads are to scale responsible for seasonal and daily peak demands in power consumption. About 20% of the power generation capacity is only used for satisfying the peak demands that occur approximately 5% of the time [3]. Reducing the peak demands and shifting the loads enables utility companies to prolong constructing new power plants. With the expanded usage of non-constant renewable energy sources, like wind and photo-voltaic energy, combined with residential battery storage systems it is possible to reduce the usage of fossil fuel and production of greenhouse gases. When integrating multiple smart homes into smart grids two demand response management schemes are being considered: Incentive-based schemes and Price-based schemes. As described in [3], when utilizing incentive-based schemes the utility company usually has some degree of direct authority over the consumed energy. While with the price-based schemes the customer gets charged for the consumed power at a varying rate which

reflects the abundance/scarcity of energy in the smart grid. This encourages the consumer to manage their loads and shift them to less congested periods.
With the future integration of smart homes into smart grids in mind, it is important to manage the electrical systems inside the residential home in an optimal way, while being subject to external smart grid constraints. In Europe a near-zero energy building standard is going to be desired by 2020 and onwards [2]. This requires local energy production to cover the residential demand. Resulting in larger residential PV areas and the usage of residential battery storage systems.
However efficient energy storage systems are currently at the research and test phase [3] thus, till now they are expensive and uneconomical. As shown in [4] it is possible to use smaller storage devices when accurate generation forecasts are available. With increased forecasting errors the capacity of the storage devices also has to increase significantly.

1.2 Problem description

Programmable thermostats in residential buildings could lead to potentially large energy savings without sacrificing user comfort, provided the setback schedules are defined correctly and unexpected events are rare [5]. Using self-learning and adaptive occupancy prediction schemes in a smart home environment those problems could be avoided. By reducing the power demand for heating only during periods without occupancy the smart home can save energy and reduce costs while keeping the residents comfortable during times they are present.
The main disturbances acting on the thermals of a building are the ambient temperature, the solar irradiation, and the occupancy. The residents do not only influence the indoor temperature via their body heat but also via usage of electronic devices. Improving predictions for those disturbances yield to more accurate control results and solutions closer to the optimum.
While weather forecasts are widely available and generally accurate, they can not account for local conditions. Buildings on one side of a slope may see lower ambient temperatures than buildings on the other side or on top. Solar irradiation might be blocked locally via trees and other obstructions. Identifying the local influences on the building also lead to more accurate predictions.
Remarkable improvements to the efficiency of electric grids can be achieved when incorporating demand side load management and end-user cooperation [6]. Thus it is advantageous to optimally manage the electrical systems of a smart home in respect to energy availability in the grid.

1.3 Research questions

The following research questions are being covered in this thesis:

Is it possible to improve the general weather forecast by using measurements taken from a weather station to form a localized prediction?

What are the formulations and benefits of a combined controller for building temperature control and electrical system management?

How does a model predictive controller for a smart home benefit from improved weather forecasts or occupancy predictions?

Chapter 2

Smart Home Model

This section deals with the modeling process of the smart home. The contents of this section represent an extension of Killian et.al. 2018 [7] which is an article submitted to the peer-reviewed journal 'Applied Energy'.
Since no two smart homes are identical, the models were kept modular. This allows for quickly adding/removing components and changing sub-systems. The smart home is represented by three models: 1) the thermal model, 2) the electrical model, and 3) the coupling node. The thermal model ensures that a certain level of user comfort is present in the smart home. It provides indoor temperature predictions based on ambient temperature, solar irradiation, and occupancy needed for the MPC-scheme. The electrical model is used to optimally manage the usage of the battery, the PV systems and the shift-able loads. The final model is the coupling node. It connects the thermal and electrical model. In this work an electrical heat pump was used as coupling element. Figure 2.1 shows the overall schematic and the connections between the sub-models.

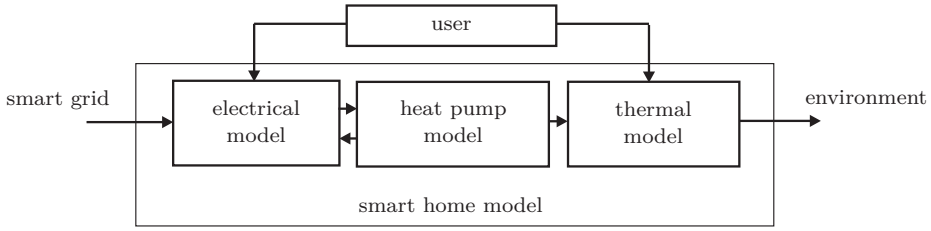

Figure 2.1: Schematic overview of the smart home model, presenting the main model components and disturbances. Figure from [7]

2.1 Thermal Model of the Smart Home

Identification and modeling of the dynamic model are usually the most difficult and time-consuming parts [8]. A second order system is chosen for the thermal dynamics of the smart home with a single temperature-controlled zone. When using lumped parameter methods for thermal modeling, 2nd order systems offer a good balance between accuracy and complexity for short-term predictions [9]. When comparing first and second-order models, [10] concluded that the latter was an improvement in terms of accuracy while only adding little additional computational effort. Both of those papers used resistance-capacitance equivalent circuits. Second-order models for buildings have been successfully parameterized with the usage of black-box methods [11]. In [12] resistance-capacitance equivalent circuits combined with the usage of AutoregRessive networks with eXogenous inputs (ARX) and non-linear ARX (NARX) networks were implemented. The second-order ARX network transformed into a state-space representation has the same structure as the model utilized in this work.
The thermal characteristics of the smart home is assumed to be an ordinary discrete linear time-invariant (LTI) state-space system given by Eqs. (2.1a) - (2.1b):

$$\boldsymbol{x}_{k+1} = \boldsymbol{A}\boldsymbol{x}_k + \boldsymbol{B}u_k + \boldsymbol{E}\boldsymbol{z}_k, \tag{2.1a}$$

$$y_k = \boldsymbol{C}\boldsymbol{x}_k. \tag{2.1b}$$

where $\boldsymbol{A} \in \mathbb{R}^{n_x \times n_x}$ is the system matrix, $\boldsymbol{B} \in \mathbb{R}^{n_x \times n_u}$ the input matrix, $\boldsymbol{C} \in \mathbb{R}^{n_y \times n_x}$ the output matrix and $\boldsymbol{E} \in \mathbb{R}^{n_x \times n_z}$the disturbance matrix. Furthermore $\boldsymbol{x} \in \mathbb{R}^{n_x}$ is the state vector, $y \in \mathbb{R}^{n_y}$ is the output vector (indoor room temperature ϑ^{act}), $u \in \mathbb{R}^{n_u}$ is the input variable (supply temperature of the heating system $\vartheta^{\text{supply}}$), and $\boldsymbol{z} \in \mathbb{R}^{n_z}$ is the input disturbance vector containing ambient temperature ($\vartheta^{\text{ambient}}$), solar irradiation and occupancy. n_x, n_u, n_y, and n_z represent the dimensions for the specific variables. The state-space system given by Eqs. (2.1a) - (2.1b) is discretized with a constant sampling time of $T_s = 15$ min. The discrete time index is denoted with $k = \{1, \ldots, T\}$, where T is the final time step.
The state-space model for the smart home represents a smart home during the heating period. The smart home consists of only one temperature controlled zone and measures the indoor temperature as well as the supply temperature of the heating system. Furthermore, a ventilation system with a heat-exchanger unit, which recovers most of the thermal energy of the exchanged air, is assumed to be implemented. This also minimizes the heat loss due to manual ventilation while making sure the humidity indoors is at a comfortable level. Note that heat losses due to open windows or doors are difficult to detect and should be avoided in any case.

2.2 Electrical Model of the Smart Home

In this section the electrical part of the smart home model is introduced. An overview of the topology is presented in Figure 2.2.

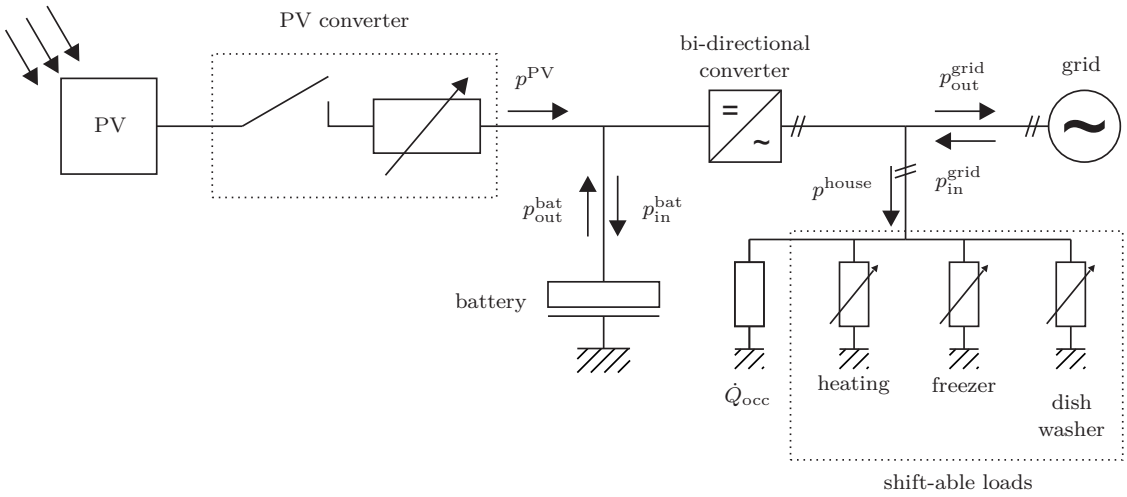

Figure 2.2: Schematic of the electrical smart home model used in this work. Figure from [7]

The following parts are implemented in the electrical model: A photo-voltaic system (PV) used for generating renewable energy for the smart home and a PV converter which generates the power output p^{PV}. Furthermore, a residential battery storage device is implemented. It is assumed that the battery can be charged with $p^{\mathrm{bat}}_{\mathrm{in}}$ or discharged with $p^{\mathrm{bat}}_{\mathrm{out}}$. The smart home is connected to a smart grid which allows it to buy the power $p^{\mathrm{grid}}_{\mathrm{in}}$ or sell the power $p^{\mathrm{grid}}_{\mathrm{out}}$ to the utility company. The total power demand p^{house} of the smart home is divided into shift-able and non-shift-able loads. The user generated load $\dot{Q}_{\mathrm{occ}}$ is the combination of all non-shift-able loads, while the shift-able loads are subdivided into heating (the power consumption of the electrical heat exchanger $p^{\mathrm{heat,\,el}}$) and the two smart appliances given as the freezer with p^{freezer} and the dish washer with p^{dishw}. The final part is the bi-directional converter, which was assumed to have perfect efficiency.

2.2.1 Overview

The combined consumed power of the smart home is given by:

$$p_k^{\mathrm{house}} = p_k^{\mathrm{user}} + p_k^{\mathrm{heat,\,el}} + p_k^{\mathrm{freezer}} + p_k^{\mathrm{dishw}}. \tag{2.2}$$

For the mathematical formulation of the global power balance in accordance to the flow directions of the power given by Figure 2.2 for any sampling time k, see Eq. (2.3):

$$\sum_{k=1}^{T}(p_k^{\mathrm{PV}} + p_{\mathrm{in},k}^{\mathrm{grid}} + p_{\mathrm{out},k}^{\mathrm{bat}}) - \sum_{k=1}^{T}(p_k^{\mathrm{house}} + p_{\mathrm{out},k}^{\mathrm{grid}} + p_{\mathrm{in},k}^{\mathrm{bat}}) = 0. \tag{2.3}$$

The energy balance for the used battery storage system is given in Eq. (2.4):

$$\mathrm{SoC}_{k+1} Q_{\max}^{\mathrm{bat}} = \mathrm{SoC}_k Q_{\max}^{\mathrm{bat}} + p_{\mathrm{in},k}^{\mathrm{bat}} \eta^{\mathrm{bat}} \Delta k - p_{\mathrm{out},k}^{\mathrm{bat}} \frac{\Delta k}{\eta^{\mathrm{bat}}}, \tag{2.4}$$

where SoC_{k+1} is the state-of-charge (SoC) at the discrete sampling time $k+1$, the maximal capacity of the battery is denoted as $Q_{\max}^{\mathrm{bat}}$, and the efficiency for charging or discharging the battery as η^{bat}. The constraints for the battery storage system are given in Eqs. (2.5a)-(2.5c):

$$\begin{aligned} \mathrm{SoC}_{\min} \leq \mathrm{SoC}_k &\leq \mathrm{SoC}_{\max}, && (2.5a)\\ p_{\mathrm{out},k}^{\mathrm{bat}} - \delta_k^{\mathrm{bat}} P_{\max}^{\mathrm{bat,\,dis}} &\leq 0, && (2.5b)\\ p_{\mathrm{in},k}^{\mathrm{bat}} - (1-\delta_k^{\mathrm{bat}}) P_{\max}^{\mathrm{bat,\,ch}} &\leq 0, && (2.5c) \end{aligned}$$

where the inequality (2.5a) defines the upper and a lower boundary for the SoC, which are $\mathrm{SoC}_{\min}$ for the lower, and $\mathrm{SoC}_{\max}$ for the upper bound. The inequalities (2.5b)-(2.5c) define a binary variable δ_k with the properties:

$$\delta_k^{\mathrm{bat}} = \begin{cases} 0 & \text{only charging is possible,} \\ 1 & \text{only discharging is possible.} \end{cases}$$

The maximum allowed discharging rate is denoted as $P_{\max}^{\mathrm{bat,\,dis}}$ and $P_{\max}^{\mathrm{bat,\,ch}}$ denotes the maximum allowed charging rate. Note that the minimum value of SoC in the battery is given by 30 % to keep some energy in the battery for unforeseen events like short power outages and also to account for prediction errors.
The PV converter can utilize power-point-tracking to convert solar-power between two limits or switch off completely. The electrical circuit equivalent to this behavior is a switch followed by a variable resistor. The mathematical formulation of these conditions can be expressed by:

$$\begin{aligned} p_k^{\mathrm{PV}} &= \delta_k^{\mathrm{conv}} (\eta_k^{\mathrm{conv}} p_{\mathrm{max},k}^{\mathrm{PV}}), && (2.6a)\\ \eta_k^{\mathrm{conv}} &\in [\eta_{\min}^{\mathrm{conv}}, \eta_{\max}^{\mathrm{conv}} \leq 1], && (2.6b) \end{aligned}$$

where $\eta_{\min}^{\mathrm{conv}}$ and $\eta_{\max}^{\mathrm{conv}}$ are the minimum and maximum converter power levels respectively. The generated power by the PV system at time instant k is denoted by $p_{\mathrm{max},k}^{\mathrm{PV}}$. The binary variable δ_k^{conv} for the converter is defined as:

$$\delta_k^{\mathrm{conv}} = \begin{cases} 0 & \text{converter is off,} \\ 1 & \text{converter is on.} \end{cases}$$

The last two variables for the power balance shown in Eq. (2.3) are based on the smart grid. In this work it is assumed that the smart grid can be represented by a perfect feedback-free drain/source of energy. Variable pricing for buying/selling from the smart grid are possible. The pricing can change hourly and future prices are know over the prediction horizon. When buying from the smart grid or selling to the smart grid, the following inequalities must hold:

$$\delta_k^{\text{grid}} p_{\text{in min},k}^{\text{grid}} \leq \quad p_{\text{in},k}^{\text{grid}} \quad \leq \delta_k^{\text{grid}} p_{\text{in,max},k}^{\text{grid}}, \tag{2.7a}$$

$$(1-\delta_k^{\text{grid}}) p_{\text{out,min},k}^{\text{grid}} \leq \quad p_{\text{out},k}^{\text{grid}} \quad \leq (1-\delta_k^{\text{grid}}) p_{\text{out,max},k}^{\text{grid}}. \tag{2.7b}$$

Note that the binary variable δ_k^{grid} is defined a:

$$\delta_k^{\text{grid}} = \begin{cases} 0 & \text{selling energy to the smart grid,} \\ 1 & \text{buying energy from the smart grid.} \end{cases}$$

The smart home can either purchase power from the grid, as long as the bought power lies between the minimum required value $p_{\text{in,min},k}^{\text{grid}}$ and the maximum allowed value $p_{\text{in,max},k}^{\text{grid}}$, or sell to the grid. The sold power must lie between $p_{\text{out,min},k}^{\text{grid}}$ and $p_{\text{out,max},k}^{\text{grid}}$ respectively. The time varying constraints introduced in Eq. (2.7a)-(2.7b) are assumed to be set by the smart grid and are known over the prediction horizon.

2.2.2 Smart Home Appliances

Two substantially different smart appliances are considered in this work: 1) the smart freezer and 2) the smart dishwasher. The first represents a variable, but continuous load while the second represents a scheduling problem.
The smart freezer is able to lower the inside temperature further than required to deep-freeze its contents. This allows the smart appliance to shift its energy demand to some degree. The freezer model is given by the LTI state-space model:

$$\vartheta_{k+1}^{\text{freezer}} = A^{\text{freezer}} \vartheta_k^{\text{freezer}} + B^{\text{freezer}} p_k^{\text{freezer}}, \tag{2.8}$$

where $\vartheta_k^{\text{freezer}}$ is the temperature inside the smart freezing unit, A^{freezer} is the system matrix and B^{freezer} is the input matrix. The actual power consumption of the freezer is denoted by p_k^{freezer}.
The constraints for the freezer are assumed to be:

$$\begin{aligned} \vartheta_k^{\text{freezer}} &\in [\vartheta_{\text{min},k}^{\text{freezer}}, \vartheta_{\text{max},k}^{\text{freezer}}], \\ p_k^{\text{freezer}} &\leq p_{\text{max}}^{\text{freezer}}, \end{aligned}$$

at every time step. The temperature constraints for the freezer are assumed to be constant and given as [-30°C, -10° C]. The maximal power consumption of the smart appliance is $p_{\max}^{\text{freezer}}$.

The smart dishwasher is constrained by a deadline which is defined as the last possible activation time. There are three different operation modes when dealing with scheduling problems. The first mode represents the dishwasher loaded and ready to start. In this mode the optimal starting point needs to be found. This mode is also the only mode that adds decision variables to the problem statement. The second mode represents the dishwasher running. During this mode the dishwasher can not be stopped and a non-constant load is consumed. The last mode represents the dishwasher being inactive.
The first mode of operation is modeled in the following way:
The duration of the dishwashers operation cycle is given by M samples. The electric power consumption profile of the M time steps is given by $\boldsymbol{L} = [L_1, L_2, \ldots, L_M]$, where L_m is the power draw at activation step m . It is assumed that N binary variables $\delta^{\text{dishw}} \in [0;1]^{1\times N}$ exist. Those binary variables are arranged in such a way that $\boldsymbol{\delta}^{\text{dishw}} = [\delta_1^{\text{dishw}}, \ldots, \delta_N^{\text{dishw}}]^{\text{T}}$. Where N is the number of possible activation points over the prediction horizon without considering the deadline. The following inequality holds: $N > M$. This is needed for the optimization problem to find the optimal solution. Defining the matrix $\tilde{\boldsymbol{L}} \in \mathbb{R}^{N\times N}$ as the lower triangular part of the toeplitz matrix of $[\boldsymbol{L},\ \mathbf{0}_{N-M}]$, or:

$$\tilde{\boldsymbol{L}} = \begin{bmatrix} L_1 & 0 & \cdots & 0 \\ L_2 & L_1 & & \vdots \\ \vdots & L_2 & \ddots & \\ L_M & \vdots & & \\ \mathbf{0} & \mathbf{0} & & 0 \end{bmatrix}, \tag{2.9}$$

allows the load for the dishwasher to be expressed by:

$$\tilde{\boldsymbol{L}}\boldsymbol{\delta}^{\text{dishw}} = \boldsymbol{p}^{\text{dishw}}. \tag{2.10}$$

The vector $\boldsymbol{p}^{\text{dishw}}$ contains N time steps of p_k^{dishw}. The constraints for the smart dishwasher are given by:

$$\sum_{k=1}^{N} \delta_k^{\text{dishw}} = 1, \tag{2.11a}$$

$$\sum_{k=k_{\text{end}}+1}^{N} \delta_k^{\text{dishw}} = 0. \tag{2.11b}$$

Where the Eq. (2.11a) enforces exactly one activation over the N time steps, and Eq. (2.11b) realizes the deadline k_{end} for the last possible activation step.

2.3 Heating System

The coupling node between the thermal model and the electrical model is given by the heat pump. This system allows the electrical system to influence the thermal system. The heat supplied to the heating system is calculated by determining the thermal heating power p^{heat} and then calculating the needed electrical power $p^{\text{heat, el}}$ via:

$$p^{\text{heat}} = \dot{m} c_p (\vartheta^{\text{supply}} - \vartheta^{\text{return}}), \tag{2.12a}$$

$$p^{\text{heat, el}} = \frac{p^{\text{heat}}}{\text{COP}}, \tag{2.12b}$$

where $\dot{m}$ represents the mass flow of the circulating water and $c_p = 4.182$ kJ/kgK the specific heat capacity of water. The supply temperature and the return temperature of the heating system are given by $\vartheta^{\text{supply}}$ and $\vartheta^{\text{return}}$ respectively. The COP or coefficient of performance is the efficiency of the heat pump. Since only the heating period is considered the inequality $\vartheta^{\text{supply}} > \vartheta^{\text{return}}$ and therefore $p^{\text{heat, el}} \geq 0$ holds true.
Note that additional heat sources such as open fire places or small wood stoves represent a considerable disturbance for the thermal model. They are difficult to model and typically no direct measurements exist. Their possible influence could be estimated by an unknown input observer, see e.g. [13].

Chapter 3

Weather Forecast

In this chapter a localized weather forecasting scheme is introduced. The section Overview deals with the motivation and problems of weather forecasts. The next two sections showcase the forecasting methods for ambient temperature and solar irradiation, respectively.

3.1 Overview

Modern numerical weather forecasting services (WFS) use discrete cells for simulating weather predictions. The initial conditions for those simulations are gathered by land based weather stations and satellite images. This results in poor localized predictions as the forecast is valid for the whole cell. The idea is to create a localized weather prediction based on the WFS and the current local sensor data.
With the usage of autoregressive models with external input (ARX) the model can learn statistically differences between local conditions (provided via the sensors) and the WFS predicted conditions.

3.2 Ambient Temperature Forecast

The WFS provides an ambient temperature prediction for the next 80 hours. In the first 65 hours hourly prediction values are available. After that the WFS only provides predictions in 3 hour intervals. An example WFS prediction for the ambient temperature can be seen in Figure 3.1.

The WFS prediction is linearly interpolated and a new time series $\vartheta_{\text{pred}}(k)$ with the uniform sampling time of $T_s = 0.25$ h is constructed. Where $k = \{1, ..., T\}$ with T being the final time step where predictions are available.

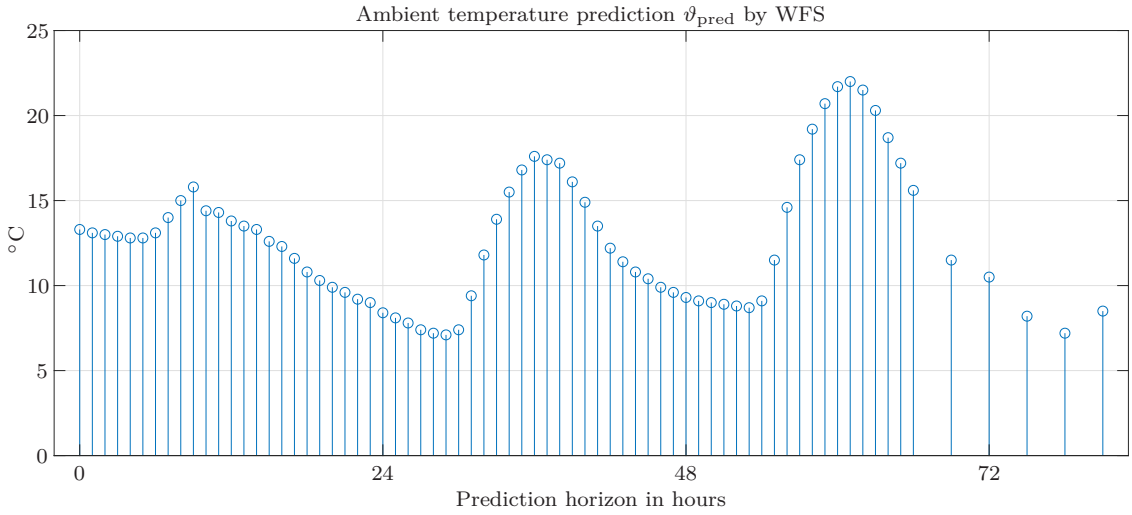

Figure 3.1: Temperature prediction from WFS. The hourly ambient temperature predictions are provided for the next 65 hours and after that in 3 h intervals for an additional 15 hours.

It is assumed that the local weather station on the smart home is measuring the local ambient temperature $\vartheta_{\text{amb}}(k)$ every 0.25 hours. The last measurements of the local temperature are saved in the system.
At every time step the vector

$$\boldsymbol{x}^T(k) = [\vartheta_{\text{amb}}(k-n+1), \ldots, \vartheta_{\text{amb}}(k), \vartheta_{\text{pred}}(k), \ldots, \vartheta_{\text{pred}}(k+m-1)] \tag{3.1}$$

is constructed, where $\vartheta_{\text{pred}}(k)$ is the latest WFS prediction for the current time step and $\vartheta_{\text{amb}}(k)$ is the current measured ambient temperature. The variables $n \in \mathbb{N}^+$ and $m \in \mathbb{N}^+$ represent the order of the denominator and nominator in the resulting ARX model.
Using the weighted recursive least squares algorithm (WRLS) shown in Equations (3.2a)-(3.2c),

$$\boldsymbol{\gamma}(k) = \frac{\boldsymbol{P}(k)\boldsymbol{x}(k)}{\boldsymbol{x}^T(k)\boldsymbol{P}(k)\boldsymbol{x}(k) + \lambda}, \tag{3.2a}$$

$$\hat{\boldsymbol{\theta}}(k+1) = \hat{\boldsymbol{\theta}}(k) + \boldsymbol{\gamma}(k)[\vartheta_{\text{amb}}(k+1) - \boldsymbol{x}^T(k)\hat{\boldsymbol{\theta}}(k)], \tag{3.2b}$$

$$\boldsymbol{P}(k+1) = \frac{1}{\lambda}[\boldsymbol{I} - \boldsymbol{\gamma}(k)\boldsymbol{x}^T(k)]\boldsymbol{P}(k), \tag{3.2c}$$

with $\boldsymbol{P}(k) \in \mathbb{R}^{(n+m)\times(n+m)}$ being the parameter-covariance matrix, $\hat{\boldsymbol{\theta}}(k) \in \mathbb{R}^{(n+m)}$ representing the estimated parameter vector, and $\boldsymbol{\gamma}(k) \in \mathbb{R}^{(n+m)}$ the correction vector.

The scalar value $\lambda \leq 1$ represents the sensitivity of the algorithm to more recent values. Choosing a λ closer to 1 will increase the amount of past samples that are significant to the current parameter estimation. With $\lambda = 1$ the WRLS algorithm will behave like a regular recursive least squares algorithm. Furthermore, $\boldsymbol{I} \in \mathbb{R}^{(n+m)\times(n+m)}$ is defined as the unity matrix.
The initial value for the parameter-covariance matrix $\boldsymbol{P}$ is chosen as $\boldsymbol{P}(0) = \alpha \boldsymbol{I}$ where $\alpha \gg 1$. The initial value for $\hat{\boldsymbol{\theta}}(0)$ is chosen as a random $(n+m) \times 1$ vector.
The future predictions for the ambient temperature, denoted by $\hat{\vartheta}_{\text{amb}}(k|j+1)$ where $j+1$ represents any given future time step and k the current time step are given by Equation (3.3). Note that $j \geq k$ and $j < T$ must hold true.

$$\hat{\vartheta}_{\text{amb}}(k|j+1) = \hat{\boldsymbol{x}}^T(k|j)\hat{\boldsymbol{\theta}}(k), \tag{3.3}$$

where

$$\hat{\boldsymbol{x}}^T(k|j) = [\tilde{\vartheta}_{\text{amb}}(k|j-n+1), \ldots, \tilde{\vartheta}_{\text{amb}}(k|j), \vartheta_{\text{pred}}(j), \ldots, \vartheta_{\text{pred}}(j+m-1)], \tag{3.4}$$

with $\tilde{\vartheta}_{\text{amb}}(k|i)$ being defined as

$$\tilde{\vartheta}_{\text{amb}}(k|i) = \begin{cases} \vartheta_{\text{amb}}(i) & \text{if } \ i \leq k \\ \hat{\vartheta}_{\text{amb}}(k|i) & \text{else,} \end{cases} \tag{3.5}$$

In Equation (3.4) $\vartheta_{\text{pred}}(j)$ is the most recent prediction for the time step j. Equation (3.5) recursively calculates predictions by calling Equation (3.3) until only current or past measurements are needed in $\hat{\boldsymbol{x}}^T$.
The predicted future values have to be recalculated after every new measurement since the parameter vector $\hat{\theta}$ is updated in Equation (3.2b).

3.3 Solar Irradiation Forecast

With the WFS providing hourly solar predictions for the next 43 hours a similar WRLS scheme as in shown in chapter 3.2 can be applied:
Instead of using the global horizontal irradiation (GHI) in W/m^2, as provided by the sensors, the clear sky index is used. The clear sky index τ_{cs} is defined by

$$G = G_{\text{cs}} \cdot \tau_{\text{cs}}, \tag{3.6}$$

where G is the current global horizontal irradiation (in W/m^2) and G_{cs} is the clear sky global horizontal irradiation (in W/m^2). The clear sky index τ_{cs} is an indication for the transmissivity of the clouds. The GHI for clear sky conditions is calculated via the

toolbox provided by Sandia National Laboratories [14].
As previously the vector

$$\boldsymbol{x}^T(k) = [\tau_{\text{cs}}(k-n+1), \ldots, \tau_{\text{cs}}(k), \tau_{\text{pred}}(k+1), \ldots, \tau_{\text{pred}}(k+m)] \tag{3.7}$$

is created at every time step $k = \{1, ..., T\}$, where T is the final time step where predictions are available and $\tau_{\text{pred}}(k+1)$ the clear sky index calculated with the WFS data. It is important to note that the current prediction $\tau_{\text{pred}}(k)$ is not used, instead the next future prediction $\tau_{\text{pred}}(k+1)$ is. This corresponds to a negative dead time. The variables $n \in \mathbb{N}^+$ and $m \in \mathbb{N}^+$ represent again the order of the denominator and numerator in the resulting ARX model.
During the day the WRLS algorithm shown in equation (3.2a) - (3.5) can be applied to compute the predictions for the clear sky index $\hat{\tau}_{\text{cs}}$. During the night no calculations are possible due to the lack of measurements. In the morning new initial values for $\boldsymbol{P}$ and $\hat{\boldsymbol{\theta}}$ are needed since the weather conditions could have changed significantly overnight.
To calculate the new initial values the latest predictions from the WFS are loaded before sunrise. This prediction is then compared against measurements from past days in a database of irradiation data.

Algorithm 1 find closest solar days

Require: $\exists\ \tau_{\text{pred},i} \in \mathbb{R}^{1\times 1}, \tau_{\text{datab}} \in \mathbb{R}^{n_d \times 48}$
  normalize τ_{pred} to 12h day $\Rightarrow \tilde{\tau}_{\text{pred}} \in \mathbb{R}^{1\times 48}$
  for $j = 1$ to n_d **do**
    $e_j = \sqrt{\frac{1}{48}\sum_i^{48}(\tilde{\tau}_{\text{pred},i} - \tau_{\text{datab},j,i})^2}$
  end for
  sort e_j ascending

The algorithm shown in Algorithm 1 outlines how to search the database (τ_{datab}) consisting of n_d normalized days for similar solar days. The 5 days corresponding to the 5 smallest values of e_j are chosen to initialize $\boldsymbol{P}$ and $\hat{\boldsymbol{\theta}}$.
For this it is assumed that the measurements in the database are the clear sky indices τ_{cs} present on those days. The latest WFS prediction τ_{pred} is assumed to be the prediction for each day. By applying the WRLS algorithm shown in equations (3.2a) - (3.2c) to those 5 days (ignoring the night phases) the new starting $\boldsymbol{P}$ and $\hat{\boldsymbol{\theta}}$ are calculated for the next day.

Bacher et.al. 2009 [15] introduced a method for online short-term predictions of solar power generation based on autoregressive models. In his work a clear sky model similar to Equation (3.6) was used with the difference that the previously cited work

proposes the usage of smoothing kernels to estimate a clear sky solar power. Furthermore, the usage of diurnal AR components is proposed. While Bacher stated that the effects of this component were only small and can be left out, it has to be noted that it implies a dependency on the weather conditions of the last day. In this work no improvement has been found by including the diurnal component.

Chapter 4

Occupancy Predictions

In this chapter the human element is introduced into the control scheme.
The first section deals with the perception of thermal comfort and what impact gender and age has on comfort needs. Furthermore, the international standard for ergonomics of the thermal environment is briefly presented. The second section showcases the occupancy prediction algorithm. Both, the off-line feature extraction and the on-line predictions are featured.

4.1 Occupancy Comfort

When designing and operating residential buildings an important boundary condition is that the thermal comfort quality must be maintained [16]. Before designing a temperature regulating scheme, the human perception of the thermal environment has to be considered.
There exists no thermal environment that can satisfy everyone due to individual differences in experiencing thermal environments [17]. While previously the differences in thermal comfort for females and males was considered insignificant, more recent studies revealed a significant gender difference [18]. While [19] found that women prefer higher room temperatures than men at home, other studies found there is no significant difference between thermal comfort requirements [18] or neutral temperature [20].
Although females become aware of thermal discomfort earlier than males [21] and express more dissatisfaction with deviations from their personal optimal thermal environment [18], males use the thermostats in households more often [19]. The last study also found that automatic control seemed to fulfill the needs of males better than the needs of females. Although, being more satisfied during the summer, females tend to feel uncomfortably cold more often during the winter season than males. It was also found that the technical knowledge of the heating systems is significantly better for males than for females, which [19] accounted to complex HVAC systems in offices and

the lower usage of thermostats by females.
Furthermore, older generations have different needs for thermal comfort compared to their younger counterparts [22]. Moreover conditions for older people may not be met if the building services are inadequately designed. J. van Hoof et.al 2017 [22] gave inadequate means for control of the preferred climate as an example for an inadequate design. There it is also concluded that 'Equipping the homes of older people with smart technologies as well as training older people to use the technology may lead to a reduced need for energy to heat or cool a space and saving operating costs'.
Furthermore are comfortable temperatures and acceptable temperature variations influenced by parameters which are often not considered by conventional methods [16]. Using improved methods for determining thermal comfort and estimating the thermal sensation of occupants will improve the resemblance with reality.
The international standard for ergonomics of the thermal environment (ISO 7730 [23]) uses predicted mean votes (PMV) and predicted percent of dissatisfaction (PPD) to predict the thermal sensations of people to thermal environments. The PMV scale is thermal comfort scale that is centered around thermal equilibrium of the human body and the environment (PMV of 0). Positive PMV values represent too warm climate, while negative values represent too cold conditions. The biggest value for PMV is +3 (hot) and the smallest value is -3 (cold). See Table 4.1.

Table 4.1: PMV values and thermal sensations

PMV	thermal sensation
+3	hot
+2	warm
+1	slightly warm
0	neutral
−1	slightly cold
−2	cool
−3	cold

When calculating the PMV various factors like air temperature, clothing factor, relative air velocity and activity have to be considered.
ISO 7730 defines furthermore the PPD as a function of the PMV. The graphical representation of PPD in dependency of PMV is given in Figure 4.1. The PPD is a non-linear measure for the thermal comfort. The smallest possible value is a PPD of 5% at PMV = 0. One advantage of using the PPD over PMV is that the scale is strictly positive for both too cold and too hot environments.

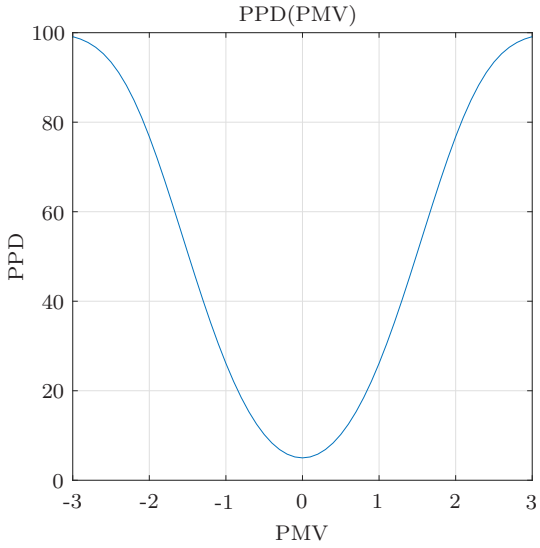

Figure 4.1: PPD as a function of PMV

4.2 Occupancy Prediction

Traditional operation practices try to maintain constant daily indoor temperature trajectories or define constraint-trajectories for minimal and maximal allowed indoor temperatures (e.g.[24]). Enforcing the indoor temperature of the smart home to always follow the set trajectory is not necessary when the resident is not at home. This would allow the smart home to save energy without decreasing user comfort.

An adaptive short-term prediction scheme was introduced in [25]. This section represents a quick overview of the algorithm used. For more details, especially about the calculations and results the reader is redirected to the original document.
The presented algorithm is self-learning and does not require prior parameterization or expert knowledge. The method is based on occupancy data which is transformed via proper orthogonal decomposition (POD) and then clustered into a low dimensional parameter space. For more information about POD or subspace parameter clustering the reader is redirected towards relevant literature like [26] and [27] respectively.

4.2.1 Off-line Feature Extraction and Clustering

Sensors in the smart home capture the occupancy status of the residents. The collected data is expressed by the matrix $\boldsymbol{X} \in \mathcal{B} = [0,1]^{N \times m}$, where N are the number of measured days and m are the collected samples per day. In this work the sampling time was chosen to be 15 minutes, therefore $m = 96$. The set $\mathcal{B}$ is the probability for occupancy.

With $r_{\max}$ being the number of significant components for the dimension reduction, the Algorithm 2 can be written as:

Algorithm 2 off-line order reduction with POD

Require: $\exists$ data matrix $\boldsymbol{X}$
Ensure: $\mathcal{B} = [0,1]^{N \times m}$
  calculate POD: $\boldsymbol{X} = \boldsymbol{U}\boldsymbol{\Sigma}\boldsymbol{V}^{\mathrm{T}}$
  find the significant components σ_i, $\forall i \in \{1, \ldots, N\}$ of the matrix $\boldsymbol{\Sigma}$, where all non-negative numbers σ_i are given as an order relation in decreasing order
  if $\sigma_{r_{\max}} = \sigma_l + \varepsilon$, $\forall l \in \{1, \ldots, N\}$ **then**
    choose $\sigma_{1,\ldots,r_{\max}}$ as significant components
  end if
  for $i = 1$ to $r_{\max}$ **do**
    calculate basis functions: $\phi_i = u_i \sigma_i v_i^{\mathrm{T}}$
    $\boldsymbol{\phi} = [\phi_1, \ldots, \phi_{r_{\max}}] \in \mathbb{R}^{m \times r_{\max}}$
  end for
  for $i = 1$ to $r_{\max}$ **do**
    calculate unknown parameters $\boldsymbol{\beta_i} = (\boldsymbol{\phi}^{\mathrm{T}}\boldsymbol{\phi})^{-1}\boldsymbol{\phi}^{\mathrm{T}}\boldsymbol{x_i}$
    $\boldsymbol{x}_i \in \mathbb{R}^{m \times 1}, \boldsymbol{x}_i \subseteq \boldsymbol{X}$
  end for

After the execution of Algorithm 2 in which the POD, which is a special singular-value decomposition, was calculated the off-line clustering described in Algorithm 3 is computed:

Algorithm 3 off-line clustering in the parameter space

Require: $\exists \beta_{j,i} \in \mathbb{R}^{1 \times 1}, \beta_{j,i} \subseteq \boldsymbol{\beta}_i$
  [cluster, $\boldsymbol{\beta}_{c_j}$] = k-means($\beta_{j,i}$)
  for $j = 1$ to r_c **do**
    calculate features: $\boldsymbol{\varphi}_j = \boldsymbol{\phi}\boldsymbol{\beta}_{c_j}$
  end for

With the centroids of the r_c clusters $\boldsymbol{\beta}_{c_j}$, the occupancy features $\boldsymbol{\varphi}_j$ can be extracted.

4.2.2 On-line Occupancy Prediction

After the possible occupancy features have been extracted in the off-line calculation the on-line predictions presented in Algorithm 4 can be computed. There the variable τ is

the actual time stamp, $\mu_{\boldsymbol{X}} = \mathbb{E}\{X_i\}$, $\forall i = \{1, \ldots, N\}$, $\mu_{\boldsymbol{\varphi}} = \mathbb{E}\{\boldsymbol{\varphi}_j\}, \forall j = \{1, \ldots, r_c\}$, and the RMSE-value is used to evaluate the fit between the individual model outputs $\hat{\boldsymbol{\varphi}}_{j,p}$ and the measured output $\boldsymbol{\varphi}_{j,p}$ over the occupancy prediction horizon, $\forall p = \{1, \ldots, n^{\text{pred}}\}$. The prediction model $\hat{\boldsymbol{\varphi}}^*$ is chosen as described by Algorithm 4. In this

Algorithm 4 on-line occupancy prediction

Require: $\exists$ features $\boldsymbol{\varphi}_j \in \mathbb{R}^{1\times m}, \forall j = \{1, \ldots, r_c\}$
  define calculation window: n^{calc}
  define prediction window: n^{pred}
  t-test statistic: $\mathcal{H}_0 : \mu_{\boldsymbol{X}} - \mu_{\boldsymbol{\varphi}} = \omega_0$; with $\alpha = 0.05$;
Require: $\boldsymbol{X}$ and $\boldsymbol{\varphi}$
  for $p = \tau$ to $\tau - n^{\text{calc}}$ **do**
    [decision $\mathcal{H}_0$, p-value] = t-test($\boldsymbol{X}_p, \boldsymbol{\varphi}_{j_p}, \alpha$), $\forall j = \{1, \ldots, r_c\}$
  end for
  for $j = 1$ to r_c **do**
    for $p = \tau + 1$ to $\tau + n^{\text{pred}}$ **do**
      $\hat{\boldsymbol{\varphi}}^* = \boldsymbol{\varphi}_{j,p}^{\max\{\text{p-value}\}} \wedge \min\{\text{RMSE}(\boldsymbol{\varphi}_{j,p}, \hat{\boldsymbol{\varphi}}_{j,p})\}$
      $\hat{\boldsymbol{\varphi}}^* \in \mathbb{R}^{1\times n^{\text{pred}}}$
    end for
  end for

work the prediction window n^{pred} for the occupancy prediction was chosen to be the same as the calculation window n^{calc}, therefore $n^{\text{pred}} = n^{\text{calc}} = 6$ h (24 samples).
For further information about the occupancy prediction, see [25].

Chapter 5

Mixed-Integer Quadratic Programming MPC

In this chapter the control schemes used in the simulations are described. The contents of this chapter represents an extension of Killian et al. 2018 [7], which is an article in the journal 'Applied Energy'. The controller has to primary ensure that the thermal requirements for user comfort are met. Secondary the controller also has to make sure the electrical systems are being used in an efficient way. This includes the decision when to charge/discharge the battery, when to buy from or sell to the grid, and when to operate the smart appliances.

5.1 Overall Control Structure

The control scheme is chosen to be a model predictive controller (MPC). The fundamental control structure is shown in Figure 5.1. The actual indoor temperature in the smart home is denoted as ϑ^{act}.

The smart home plant model was described in chapter 2. The manipulated variables $\boldsymbol{u}^*$ consists of the inputs for the electrical plant (binary and continuous variables) and the inputs for the heat pump (heat supply temperature).

Table 5.1 gives an overview of the controlled variables, manipulated variables and disturbances. Where semi-continuous variables describe variables that are continuous under certain discrete conditions. For example the battery can be charged continuously when the discrete condition ($\delta_k^{\mathrm{bat}} = 0$) is satisfied. Otherwise charging is prohibited and only discharging is possible.

The external inputs for the mixed integer quadratic programming (MIQP)-MPC are the occupancy prediction $\hat{\boldsymbol{\varphi}}^*$ described in chapter 4, the weather forecasts, the user preferences expressed as weighting factors, the preferred reference temperature trajec-

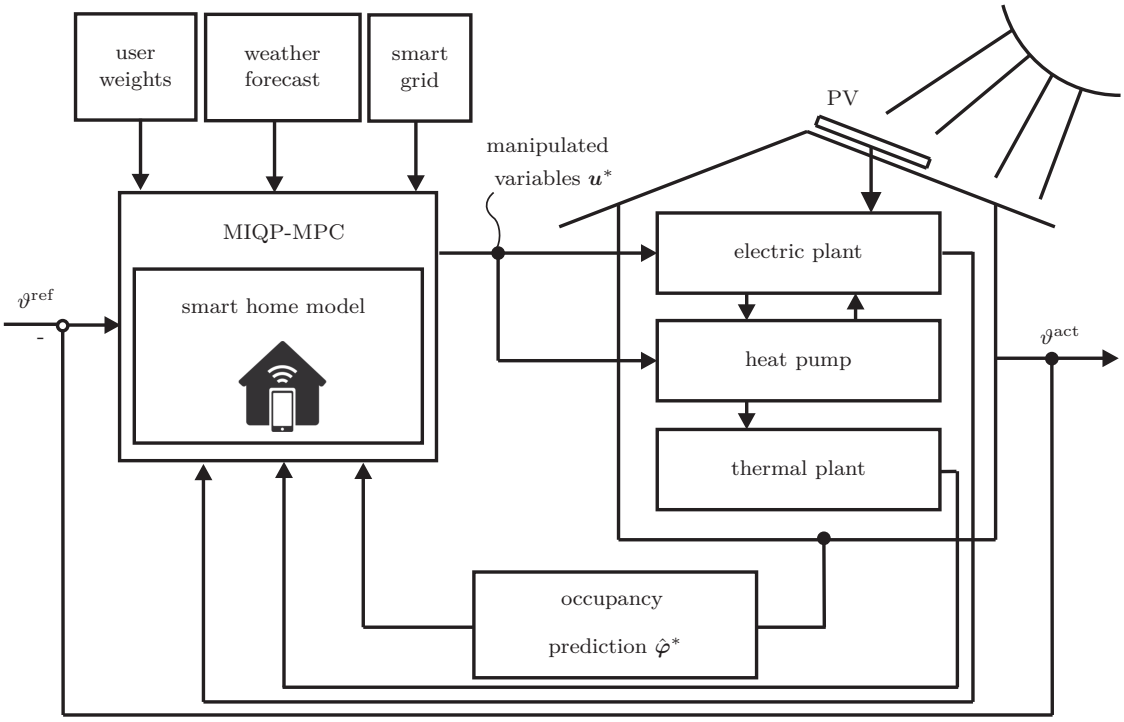

Figure 5.1: Schematic control structure of the smart home and MPC . Figure from [7].

tory, and the prices as well as constraints of the smart grid. The user is tasked to find an trade-off between comfort ($\mathcal{Q}$), monetary cost ($\mathcal{S}$), and energy efficiency ($\mathcal{P}$), which is represented in the global optimization criteria via weighting factors.

5.2 MIQP Cost Function

The global optimization criteria is given by Eqs. (5.1a)-(5.1e).

$$J^* \equiv J(\boldsymbol{u}^*) = \min_{\Delta \boldsymbol{u}} J(\boldsymbol{u}), \tag{5.1a}$$

where

$$\begin{aligned} J(\boldsymbol{u}) \quad &= \quad \sum_{k=0}^{n_p} [(\vartheta_k^{\text{ref}} - \vartheta_k^{\text{act}})' \mathcal{Q}_k (\vartheta_k^{\text{ref}} - \vartheta_k^{\text{act}}) \\ &+ \quad \Delta \boldsymbol{u}_k{}' \mathcal{R}_k \Delta \boldsymbol{u}_k + (g_k^{\text{buy}} \mathcal{S}_k + \mathcal{P}_k) p_{\text{in},k}^{\text{grid}} \\ &- \quad g_k^{\text{sell}} \mathcal{S}_k p_{\text{out},k}^{\text{grid}}], \end{aligned} \tag{5.1b}$$

subject to

Table 5.1: List of controlled and manipulated variables as well as disturbances of the MPC

controlled variable	indoor room temperature ϑ^{act}
manipulated variables	
continuous	heat supply temperature $\vartheta^{\text{supply}}$
	PV converter power point tracking η_k^{conv}
	smart freezer power consumption p_k^{freezer}
semi-continuous	buying/selling from the grid $p_{\text{in},k}^{\text{grid}}$ / $p_{\text{out},k}^{\text{grid}}$
	battery charging/discharging $p_{\text{in},k}^{\text{bat}}$ / $p_{\text{out},k}^{\text{bat}}$
discrete	smart dishwasher activation point $\boldsymbol{\delta}^{\text{dishw}}$
	PV converter on/off δ_k^{PV}
disturbances	occupancy (acting on thermal and electrical part)
	ambient temperature ϑ^{amb}
	solar irradiation (acting on thermal and via PV on electrical part)
	grid prices and constraints

$$\text{Eqs. (2.3)} - \text{(2.12b) from Chapter 2,}$$

$$\Delta u_{1,k}, \in [-5°\text{C}, 5°\text{C}], \tag{5.1c}$$

$$u_{1,k}^* \in [26°\text{C}, 50°\text{C}], \tag{5.1d}$$

$$\vartheta_k^{\text{act}} \in [\vartheta_{\text{min},k}^{\text{act}}, \vartheta_{\text{max},k}^{\text{act}}]. \tag{5.1e}$$

With the first element of $\boldsymbol{u}_k^*$, denoted as $u_{1,k}^*$, being defined as the heat supply temperature $\vartheta_k^{\text{supply}}$. The constraints in Eq. (5.1d) are designed for the heating period only. An easy adaption for cooling in the summer is possible. The minimum and maximum indoor temperature constraints (5.1e) are time-varying and dependent on the occupancy prediction. If occupancy is predicted the absolute difference between the constraints and the set reference temperature ϑ_k^{ref} gets smaller. If no occupancy is predicted the gap between ϑ_k^{ref} and the allowed lower/upper constraint is bigger. Note that the indoor room constraints in Eq. (5.1e) are modeled as soft-constraints to ensure feasibility of the optimization problem.

In the definition of the cost function in Eq. (5.1b) the prediction horizon of the MIQP-MPC is denoted as n_p. In the chosen formulation the control horizon is the same as the prediction horizon. Also seen in this equation are the user-chosen weighting matrices: $\mathcal{Q}_k$ is the matrix to weight the user comfort, $\mathcal{R}_k$ is the penalize-matrix for the manipulated variables, the matrix $\mathcal{S}_k$ weights the cost for buying from the smart grid

and therefore represents operating costs, the matrix $\mathcal{P}_k$ is the weight for the energy efficiency to minimize energy bought from the grid and therefore maximizing the usage of the internal renewable energy source. The variable prices for buying and selling from the smart grid are given as g_k^{buy} and g_k^{sell} respectively. The power consumed from the smart grid is given as $p_{\text{in},k}^{\text{grid}}$, and the power sold to the smart grid is denoted by $p_{\text{out},k}^{\text{grid}}$.

5.3 User Weights

As described in the previous section the user is tasked to balance the weighting matrices in Eq. (5.1b). Usually the end-user lacks the technical knowledge to do this in an efficient manner. Therefore an easy to use scheme is presented to allow the users to balance their individual preferences. The overall performance of the smart home MIQP-MPC is a trade-off between three conflicting goals: 1) to provide the best possible user comfort, 2) to minimize the operating costs, and 3) to spend as little external energy as possible. These goals are represented by the weights $\mathcal{Q}$, $\mathcal{S}$, and $\mathcal{P}$ respectively. The individual corners of the proposed interface shown in Figure 5.2 represent those goals.

The user is now tasked to select a point inside the triangle. The closer the point is

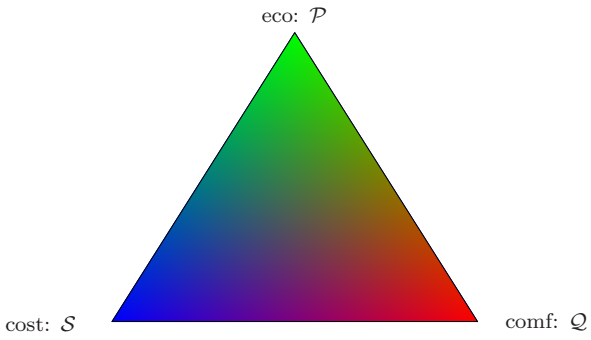

Figure 5.2: Interface for the user to choose their individual weights. Figure from [7]

to one of the corners the more the respective goal is prioritized by the controller. By mapping the coordinates of the chosen point, represented by barycentric coordinates, into the weighting factors it is possible to visually balance the conflicting goals.
The weights in the corners were a priori chosen by the manufacturer to ensure smooth operation.

5.4 Mixed-Integer Solver

Traditional MPC problems usually have a quadratic or linear cost function and linear constraints in the form of $\boldsymbol{lb} \leq \boldsymbol{A} \cdot \boldsymbol{x} \leq \boldsymbol{ub}$, where $\boldsymbol{x} \in \mathbb{R}^{n_x}$ is the decision variable vector, $\boldsymbol{A} \in \mathbb{R}^{n_b \times n_x}$ is the linear constraint matrix, $\boldsymbol{lb} \in \mathbb{R}^{n_b}$ and $\boldsymbol{ub} \in \mathbb{R}^{n_b}$ are the lower and upper bounds respectively. Note that n_b denotes the amount of boundary conditions and n_x the amount of decision variables. Therefore a quadratic programming (QP) solver is usually suitable.
The proposed controller utilizes binary decision variables in the formulation in addition to continuous decision variables, see Table 5.1. This renders the problem non-convex and mathematically difficult to solve. For algorithms to still be able to solve those kind of problems efficiently methods like branch-and-bound [28], branch-and-cut [29] or cutting planes [30] have to be used. The used solver for the mixed-integer-problem (MIP) was Gurobi 7.5.2. Gurobi supports 17 different types of cutting planes, 14 different MIP feasibility heuristics, symmetry detection, parallel branch-and-cut, and non-traditional tree-of-tree searches in the current version[31]. This allows the solver to converge to the optimal solution quickly and reliable.

Chapter 6

Results

6.1 Overview

In this chapter the simulation setups as well as the results of this work are presented. The section 6.2 showcases the introduced localized weather forecasting scheme. The section 6.3 deals with the simulation setup and results of the MIQP-MPC scheme proposed in Chapter 5. The impacts of the localized weather prediction on the performance of the controller can be seen in section 6.4. For the results of the occupancy prediction algorithm presented in Chapter 4 the reader is referred to Killian et al.2018 [25].

6.2 Weather Forecast

In this section the results of the localized weather forecast algorithms described in Chapter 3 will be shown.
Both ambient temperature and solar irradiation forecasting simulations use data collected over a period of 36 days. The smart home's weather station collects measurements for ambient temperature (in deg C) and solar irradiation (in W/m^2) hourly. The solar measurements are available for each of the cardinal directions. All measurements were linearly interpolated to a common sampling time of 15 minutes.

6.2.1 Ambient Temperature Forecast

The values for n and m in (3.1) represent the order of the ARX model. The denominator-order is set by n and represents how many past measurements are used in the model. The numerator order is defined by m and corresponds to the amount of future predictions used.
Since the ARX model represents a stochastic system rather than a physical system no correct model order can be determined. The optimal order for the model was de-

Table 6.1: Parameters used for the ambient forecast

Variable	Value
Np	96 Samples = 24 hours
n	1
m	2
λ	0.995

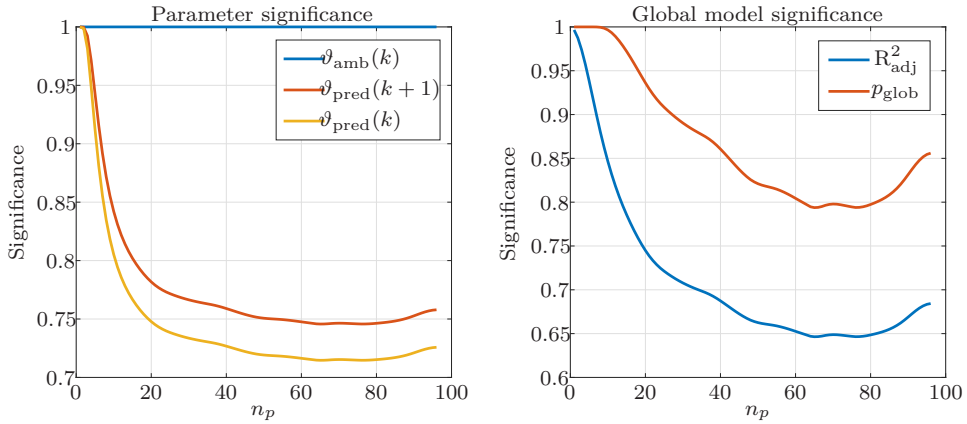

Figure 6.1: Parameters significance and global model significance over the prediction horizon for ambient forecasting

termined by testing the global significance of the model and the significance of the individual parameters and choosing the values that offer the best trade-off between them. The parameters used for the simulation can be found in Table 6.1. In the right plot of Figure 6.1 the adjusted coefficient of determination R^2_{adj} and a global F-Test with p_{glob} being the probability that at least one value of $\hat{\boldsymbol{\theta}}(k) \neq 0$ are shown over the prediction horizon n_p for the chosen parameters. Furthermore the results of the t-test for parameter significance over the prediction horizon n_p can be seen in the left plot of Figure 6.1.

In the Figure 6.2 a comparison of the ARX model predictions $\hat{\vartheta}_{\text{amb}}$ and the WFS predictions ϑ_{pred} over a sample 7 day interval are shown. The black dash-dotted line represents the real temperature ϑ_{amb} measured by the sensor. The ARX model predictions are the outputs after a long enough period of time for the parameters to settle down.

To show that the WFS in Figure 6.2 does not simply have a static offset, a zero order ARX model with the output $\hat{\vartheta}_{\text{zero}}$ was calculated. This was done by setting $\boldsymbol{x}^T$ in

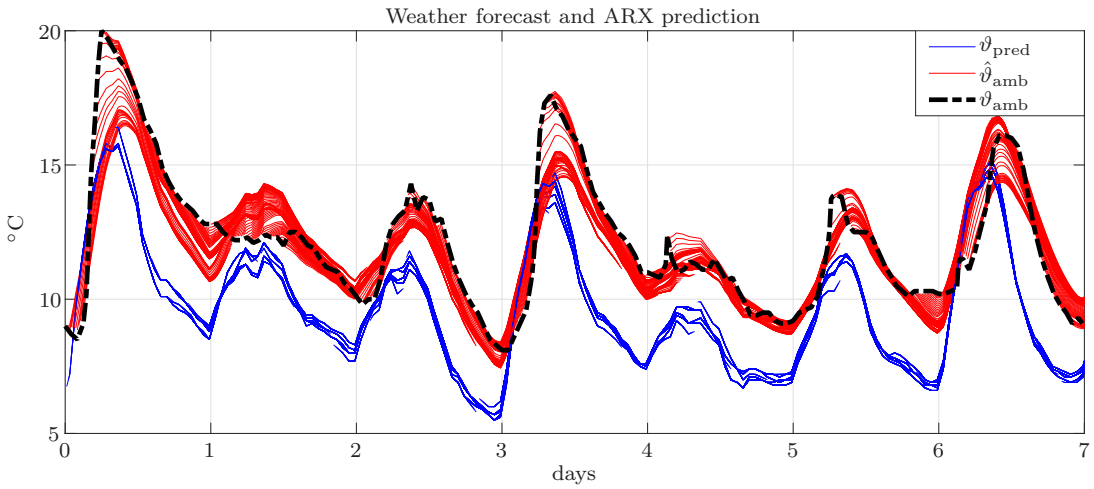

Figure 6.2: 7 day interval of WFS and ARX-Model output for ambient forecasting

Equation (3.1) to $\boldsymbol{x}^T = 1$. The rest of the algorithm stays the same. After a run-in period the different RMSE over the prediction horizon are compared. This can be seen in Figure 6.3. The RMSE between two variables is defined as the root mean square error, or:

$$\text{RMSE}(\vartheta_{\text{amb}}, \hat{\vartheta}_{\text{amb}}) = \sqrt{\frac{1}{K}\sum_{k=1}^{K}(\vartheta_{\text{amb}}(k) - \hat{\vartheta}_{\text{amb}}(k))^2} \tag{6.1}$$

The RMSE for the WFS, $\text{RMSE}(\vartheta_{\text{amb}}, \vartheta_{\text{pred}})$, is fairly constant at 3°C over the whole prediction horizon. For short term predictions the ARX model and the zero order model create good results. While the ARX model stays constant with a $\text{RMSE}(\vartheta_{\text{amb}}, \hat{\vartheta}_{\text{amb}})$ of about 1.5°C, the $\text{RMSE}(\vartheta_{\text{amb}}, \hat{\vartheta}_{\text{zero}})$ increases until it even surpasses the WFS between $30 \leq n_p \leq 65$. The reason for the $\text{RMSE}(\vartheta_{\text{amb}}, \hat{\vartheta}_{\text{zero}})$ to decline at higher n_p values is because of the daily recurring variations in temperature during the day.

6.2.2 Solar Irradiation Forecast

As seen in subsection 6.2.1, the optimal values for n and m were evaluated by examining the parameter significance and the global model significance. The chosen simulation parameters can be found in Table 6.2. The results for parameter and global mode significance for the chosen parameters are visualized in Figure 6.4. It has to be noted that the rising significance over the prediction horizon n_p is caused by the fact that the amount of samples, which can be used for long-term predictions are decreasing due to

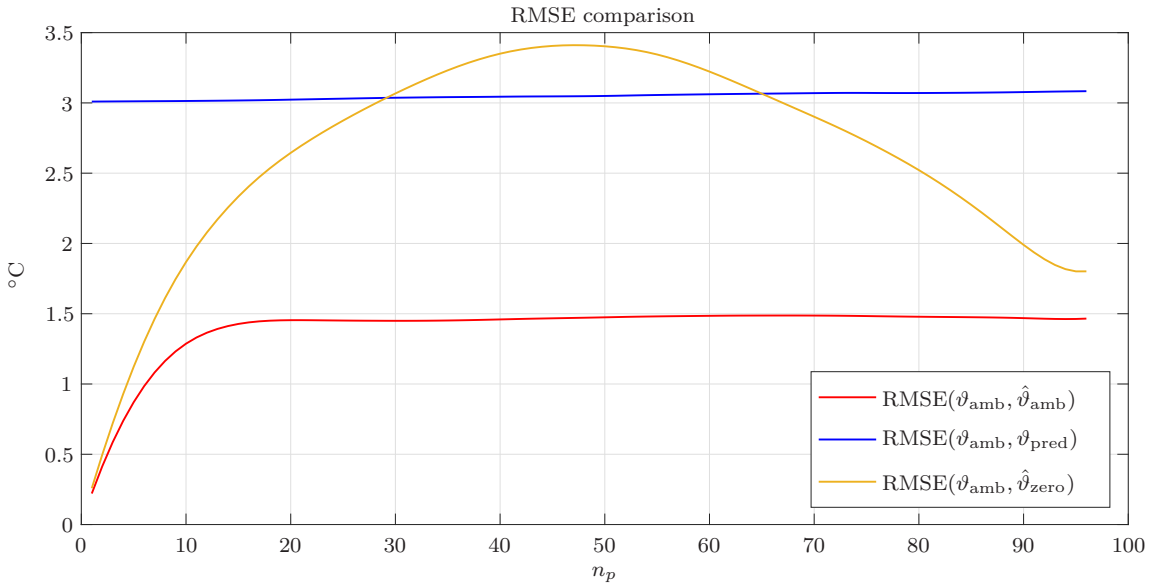

Figure 6.3: RMSE between the ARX-Model output, the WFS and the zero-order model for ambient forecasting

sunset.

Table 6.2: Parameters used for the solar forecast

Variable	Value
Np	till sunset
n	1
m	3
λ	0.98

In Figure 6.5 the ARX model output $\hat{\tau}_{cs}$ and the WFS predictions τ_{pred} can be seen for 4 selected days. The black dash-dotted line represents the real (measured) clear sky index τ_{cs}. During the start/end of the sunny days the value for the clear sky index τ_{cs} is bouncing around. This is due to the small magnitudes of solar irradiation measured and also small magnitudes of clear sky solar irradiation G_{cs} computed which leads to unstable estimations. During the day, when the clear sky index settles down, the predictions are stable. In Figure 6.6 the outputs have been converted to GHI in W/m^2.

A zero-order model is introduced by setting $\boldsymbol{x}^T = 1$ in Equation (3.1). The predictions of the zero-order model are denoted by $\hat{\tau}_{zero}$. The RMSE values of the ARX model

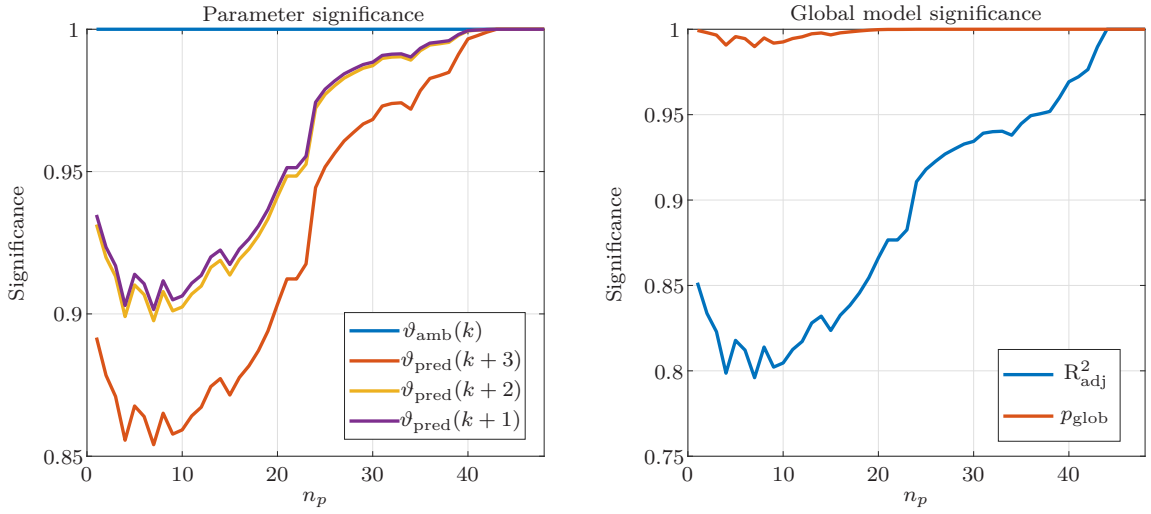

Figure 6.4: Parameters significance and global model significance over the prediction horizon for solar forecasting

prediction RMSE($\tau_{\text{cs}}, \hat{\tau}_{\text{cs}}$), the WFS prediction RMSE($\tau_{\text{cs}}, \tau_{\text{pred}}$), and the zero-order model RMSE($\tau_{\text{cs}}, \hat{\tau}_{\text{zero}}$) can be seen in Figure 6.7. The prediction of the clear sky index yields a similar behavior to the ambient temperature prediction:
The zero-order model and the ARX model provide good short time predictions. While previously the ARX and WFS models produced constant results, this time the error grows over the prediction horizon. The difference between ARX and WFS predictions is smaller, but the ARX produces still better results than WFS over the whole horizon.

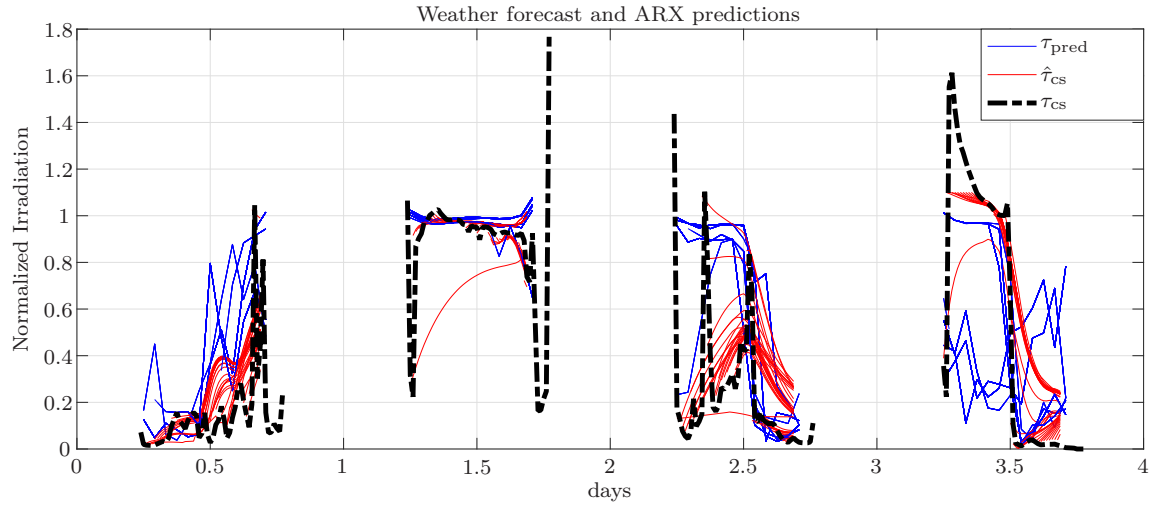

Figure 6.5: Comparison of normalized WFS and ARX-Model output for solar forecasting on 4 selected days

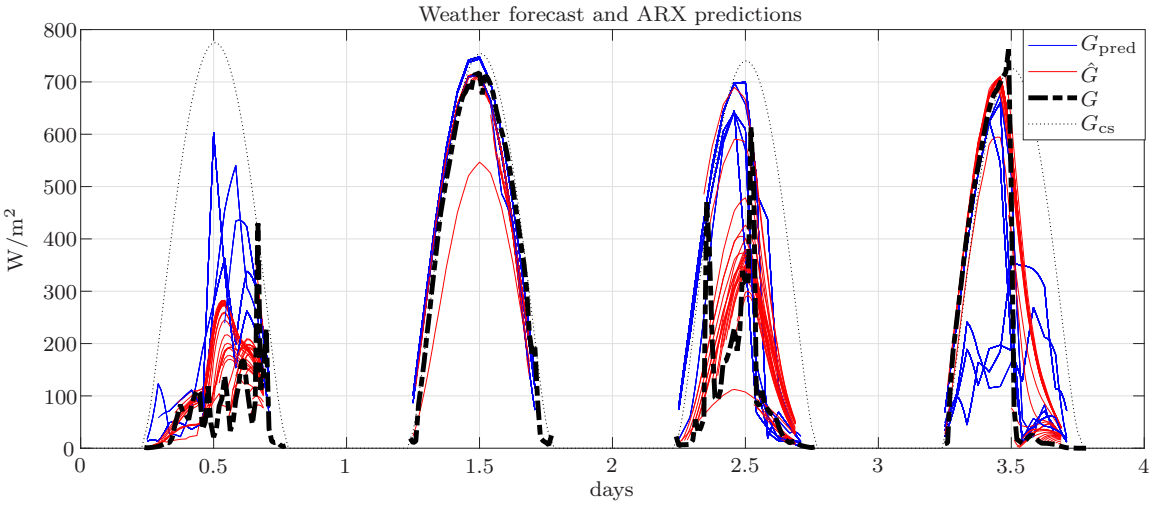

Figure 6.6: Comparison of WFS and ARX-Model output for solar forecasting on 4 selected days

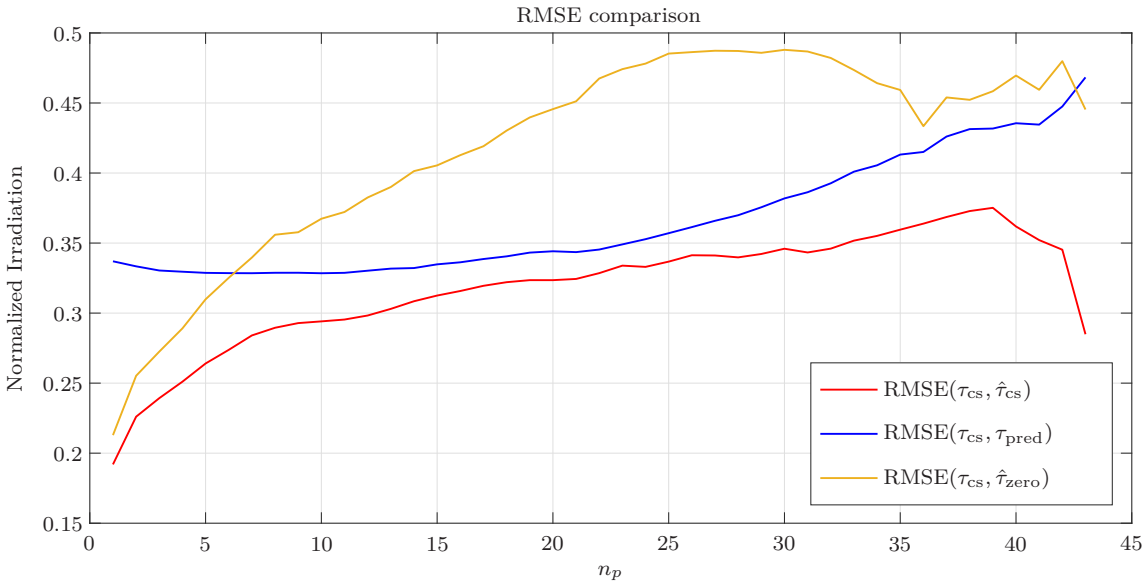

Figure 6.7: RMSE between the ARX-Model output, the WFS and the zero-order model for solar forecasting

6.3 MIQP-MPC

The smart home model presented in Chapter 2 is used for the simulations in combination with the MIQP-MPC proposed in Chapter 5. The solver applied to the MIQP-problem is Gurobi 7.5.2, see [31]. Until noted otherwise the parameters shown by Table 6.3 are used in the simulations.

Table 6.3: Simulation parameters

variable	value
T_{sim}	7 days
sampling time k	15 min
dishwasher	1 activation per 2$^{\text{nd}}$ day
	$\boldsymbol{L} = [2, 0.5, 0.5, 1]$ kW
COP	3.7
$\dot{m}$	0.1025 kg·s^{-1}
$\vartheta^{\text{return}}$	26°C
$Q_{\text{max}}^{\text{bat}}$	6.54 kWh
$P_{\text{max}}^{\text{bat, dis}}$	2.3 kW
$P_{\text{max}}^{\text{bat, ch}}$	3.0 kW
$P_{\text{max}}^{\text{PV}}$	4.5 kW at STC [32]
SoC_{min}	30 %
SoC_{max}	95 %
$\text{SoC}_{k=0}$	90 %
$\eta_{\text{min}}^{\text{conv}}$	10 %
$\eta_{\text{max}}^{\text{conv}}$	100 %
η_{bat}	0.935
n_p	96 samples = 24 h

The predictions for the ambient temperature and the solar irradiation are provided by weather services and do not utilize the localization scheme presented in Chapter 3. The smart home is assumed to possess a weather station and therefore can measure the current ambient temperature and the current solar irradiation. It is further assumed that the smart home incorporates various sensors to detect occupancy reliably and the occupancy prediction scheme shown in Chapter 4 outputs predictions for the next 6 h. Since the prediction horizon n_p with 24 hours is longer than the occupancy prediction, the last value of the prediction is continued till the end n_p. Likewise it is assumed that

the indoor temperature ϑ^{act} is being measured.
The occupancy generated load $\dot{Q}_{\text{occ}}$ is based on the average residential power consumption during the day and is assumed to be known over the prediction horizon [33].
The soft constraints for the indoor temperature are dependent on the occupancy prediction $\hat{\varphi}^*$ and given by the following equations:

$$\vartheta^{\text{act}}_{\text{min},k} = \vartheta^{\text{ref}}_k - (-5\hat{\varphi}^*_k + 5), \tag{6.2a}$$
$$\vartheta^{\text{act}}_{\text{max},k} = \vartheta^{\text{ref}}_k + (-4\hat{\varphi}^*_k + 5), \tag{6.2b}$$

where a value of 0 for $\hat{\varphi}^*_k$ means no occupancy and $\hat{\varphi}^*_k = 1$ means certain occupancy.
The user comfort will be expressed via two metrics. The first metric represents the temperature RMSE(ϑ^{ref}_p, ϑ^{act}_p) where p are all the time steps where the smart home is occupied. The second metric is defined by the predicted percentage of dissatisfaction (PPD), which is a measurement for thermal discomfort, see Section 4.1 or [23]. It is important to note that the PPD also depends on various factors like activity, clothing and air velocity. Those parameters were chosen in such a way that maximal user comfort was achieved at the set indoor temperature ϑ^{ref}. It has to be further noted that the smallest value for the PPD is 5%. The average PPD (aPPD) represents the average of all the PPD values when the smart home was occupied.

6.3.1 Performance Modes Comparison

As shown in Section 5.3, the end-users can tune their individual controller by balancing between the 3 modes 'comf', 'eco' and 'cost'. The different behavior for each performance mode is presented in this subsection.

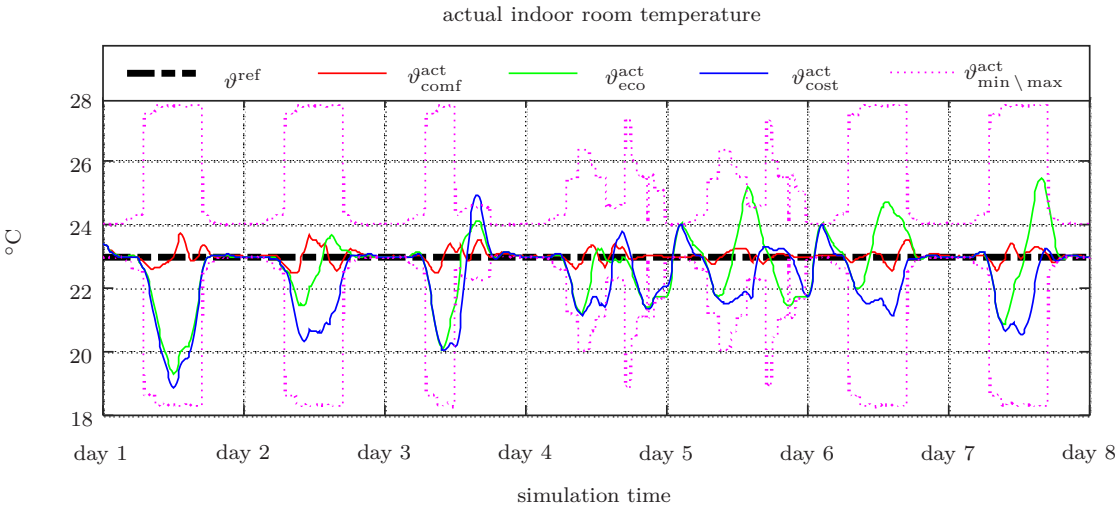

Figure 6.8: Comparison of the indoor room temperature of different controller weights. Note that the notation "day 1" represents the first day of simulation at 00:00. Figure from [7].

Figure 6.8 showcases the different resulting indoor temperatures ϑ^{act} for each MIQP-MPC performance case. All cases have the same reference set-point ϑ^{ref} of 23°C. The upper and lower soft constraint temperatures $\vartheta^{\mathrm{act}}_{\mathrm{min,max}}$ for the indoor temperature ϑ^{act} are also chosen to be the same among all cases and are given by the Equations (6.2a)-(6.2b).
As desired, the indoor temperature of the 'comf' mode ($\vartheta^{\mathrm{act}}_{\mathrm{comf}}$) is tracking the reference temperature all the time, while the other two cases ('eco' mode $\vartheta^{\mathrm{act}}_{\mathrm{eco}}$ and 'cost' mode $\vartheta^{\mathrm{act}}_{\mathrm{cost}}$) are reducing the indoor temperature ϑ^{act} during times without occupancy. While the 'cost' mode is selling all surplus energy to the grid, the 'eco' mode is utilizing the thermal mass of the smart home by over-heating the rooms during times of energy excess. This over-heating of the smart home enables the controller to use the thermal mass of the smart home as an additional energy storage.
The differences between the 'eco' and 'cost' mode are visualized in detail in Figures 6.9 and 6.10. There the upper subplots showcases the different power-sources as positive values (generated PV power, buying from grid, discharging the battery) and power-sinks as negative values (selling to grid, charging the battery and operating the smart appliances). The 'cost' mode features substantially more power sold to the grid (negative values of grid) and uses the battery to buy power from the grid when the price is at the lowest. In the lower subplots the SoC of the battery over the simulation time is shown.

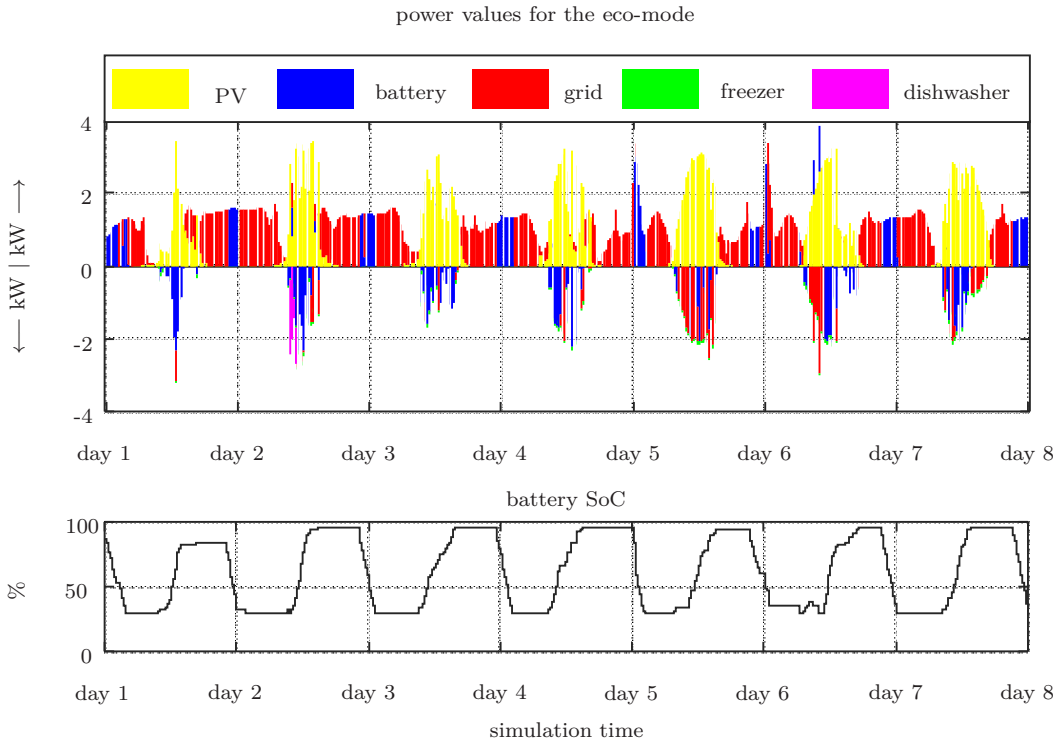

Figure 6.9: Illustration of the energy management system for the **eco-mode**. Figure from [7].

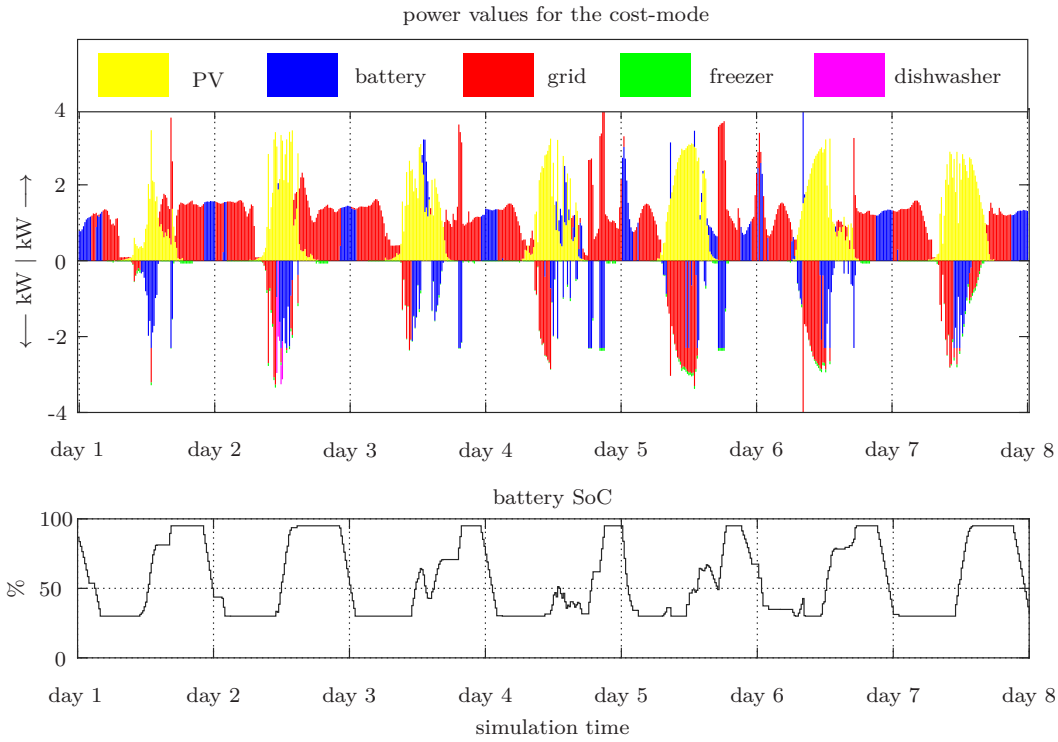

Figure 6.10: Illustration of the energy management system for the **cost-mode**.

The disturbances acting on the system during the simulations are presented in Figure 6.11 as well as the applied control variables for each case. Note that the plotted ambient temperature, solar irradiation and occupancy are the actual values acting on the system and not the predictions for the MIQP-MPC.

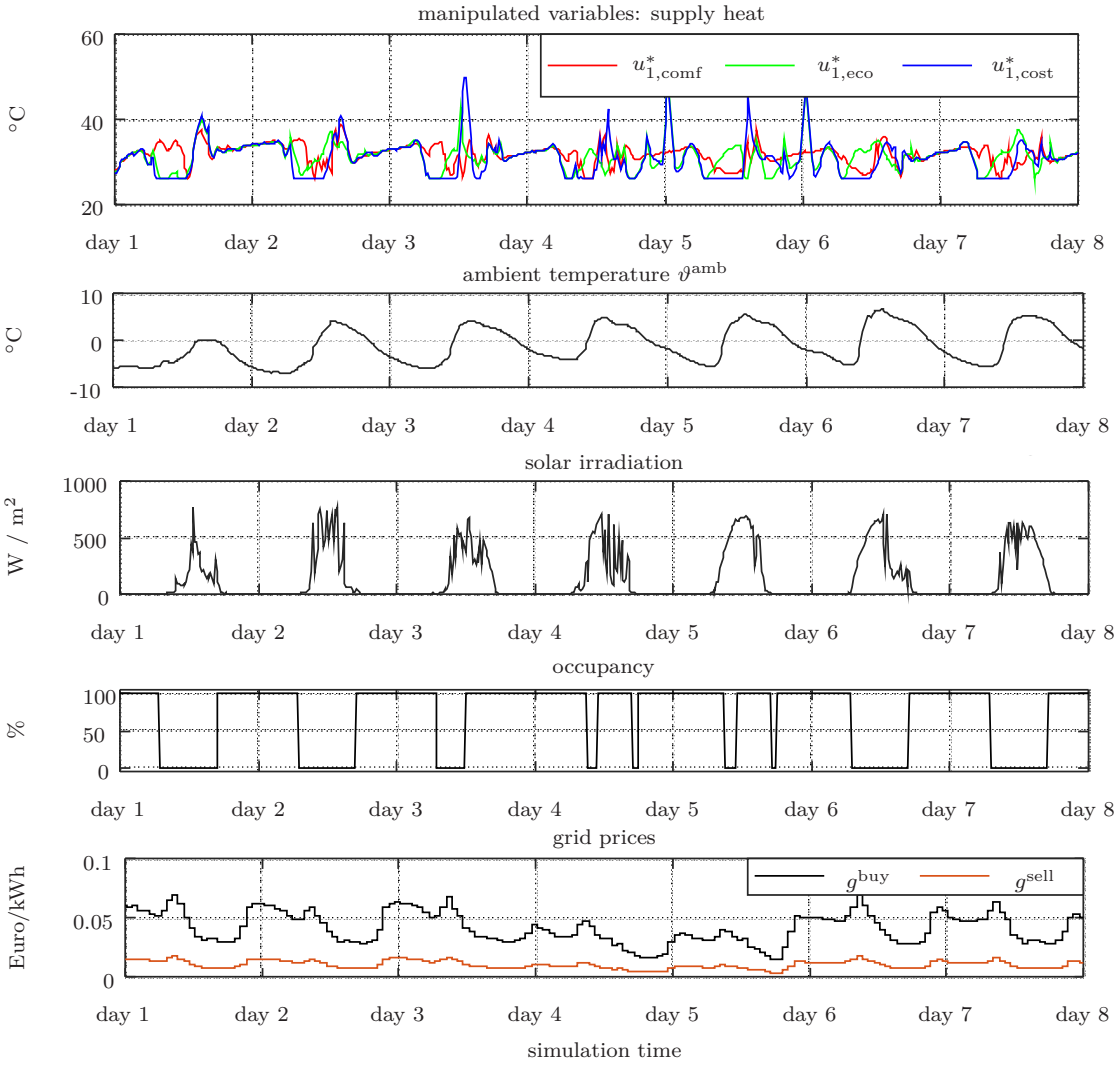

Figure 6.11: Manipulated variables and disturbances during the 7 day simulation case, related to Fig. 6.8. Figure from [7].

The performance numbers of the different modes are given in Table 6.4. Furthermore, another mode called 'center' is introduced which represents the case of choosing the geometric center in Figure 5.2.

Table 6.4: Performance modes comparison for 7 days

mode	operating cost	grid energy	average PPD	RMSE(ϑ_p^{ref}, ϑ_p^{act})
comf	4.54 €	123 kWh	5.12 %	0.19° C
eco	3.88 €	101 kWh	5.77 %	1.05° C
cost	3.72 €	110 kWh	5.91 %	1.24° C
center	4.06 €	109 kWh	5.31 %	0.54° C

The results from Table 6.4 can also be seen in the spider diagram illustrated by Figure 6.12. Note that the center of this diagram represents the best trade off between the metrics. Curves with larger inside area represent worse performance. Unsurprisingly the 'comf' mode has the lowest aPPD value while the 'cost' mode is the most cost efficient and the 'eco' mode consumes the least energy. Both the 'eco' and the 'cost' cause approximately the same thermal discomfort. The 'center' mode is a trade off between all the performance metrics.

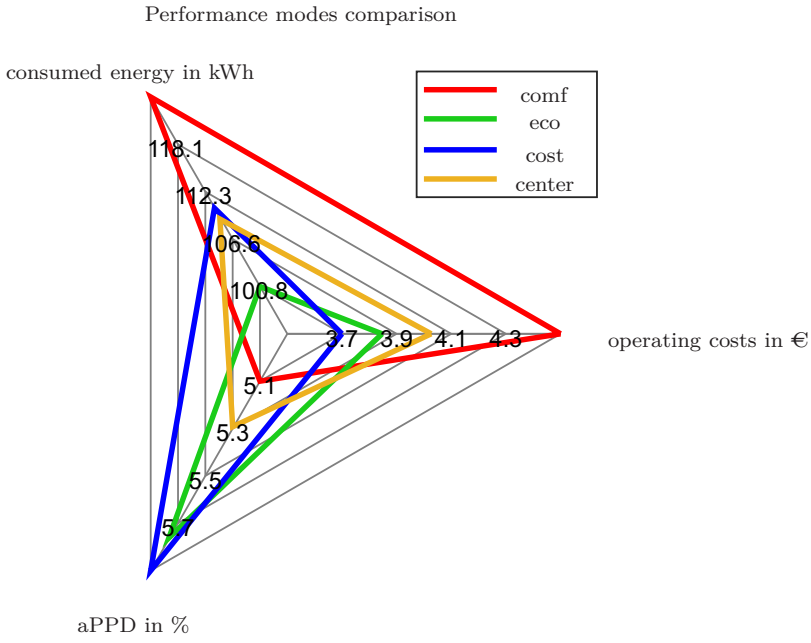

Figure 6.12: Performance of the different modes over 7 days from Fig. 6.8. Figure from [7].

6.3.2 Smart Grid Power Constraints

The smart grid can impose load constraints on the smart home by changing the values of $p^{\text{grid}}_{\text{in,min},k}$, $p^{\text{grid}}_{\text{out,min},k}$, $p^{\text{grid}}_{\text{in,max},k}$ and $p^{\text{grid}}_{\text{out,max},k}$ where setting any of the minimal variables

to nonzero values would force the smart grid to either consume or provide power to the smart grid. On the other hand when any of the maximal variables are set to zero the smart home cannot buy from the smart grid ($p^{\text{grid}}_{\text{in,max},k} = 0$) or sell to the smart grid ($p^{\text{grid}}_{\text{out,max},k} = 0$).
In the following simulation it was assumed, that the smart grid requests the smart home to not consume any power during a 4h night period starting at 00:00 on the second day by setting $p^{\text{grid}}_{\text{in,max},k} = 0$. The smart home was informed of that constraint well in advance.

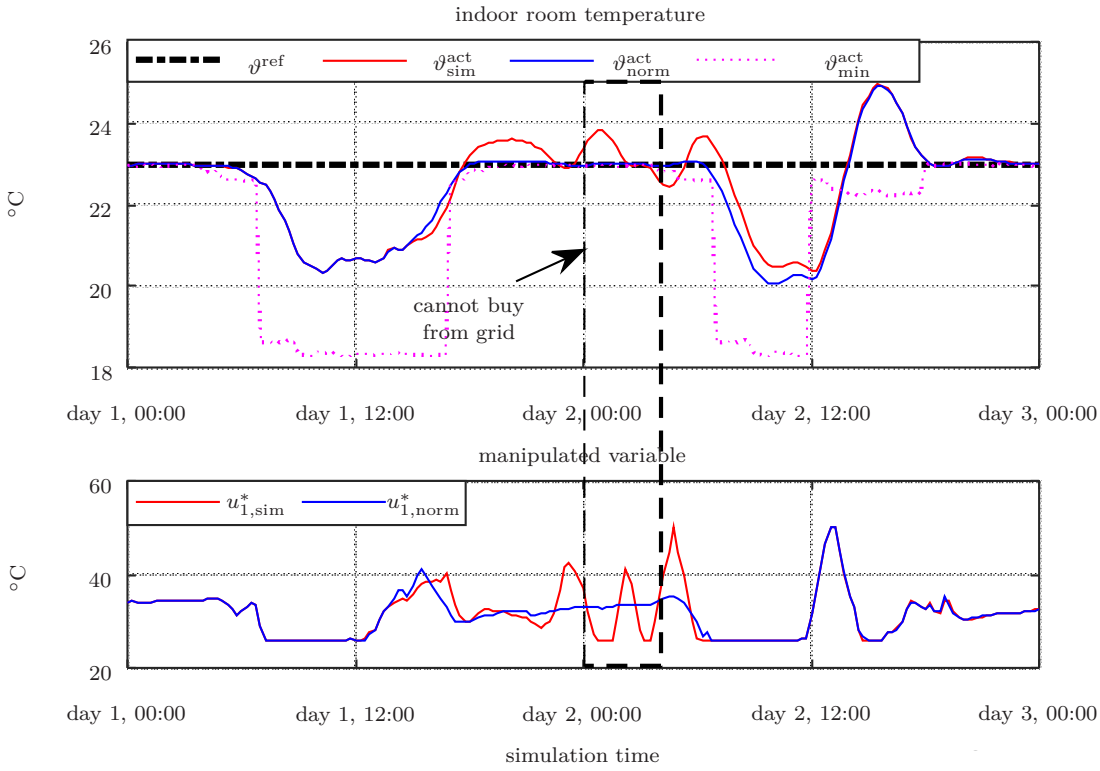

Figure 6.13: Thermal impact of grid-side load constraints. Figure from [7].

In Figure 6.13 the difference between the indoor temperature between the case with load constraint ($\vartheta^{\text{act}}_{\text{sim}}$) and without load constraint ($\vartheta^{\text{act}}_{\text{norm}}$) can be seen. In both cases the MIQP-MPC was in the 'cost' mode. Before the load constraint is enforced the controller over-heats the smart home to minimize the energy expense during the time the battery has to be used. The violation of the lower soft constraint on the second day at 12:00am is not caused by the load constraint, but rather by the occupancy prediction not expecting the user to return so early.
The responses of the electrical systems are presented in Figure 6.14. Comparing the

top two plots, the energy demand is shifted to before and after the grid-side load constraint. The bottom graph shows how the SoC of the battery system is affected by the constraint. Where SoC_{sim} represents the state of charge in the case with load constraint and SoC_{norm} the case without load constraints.

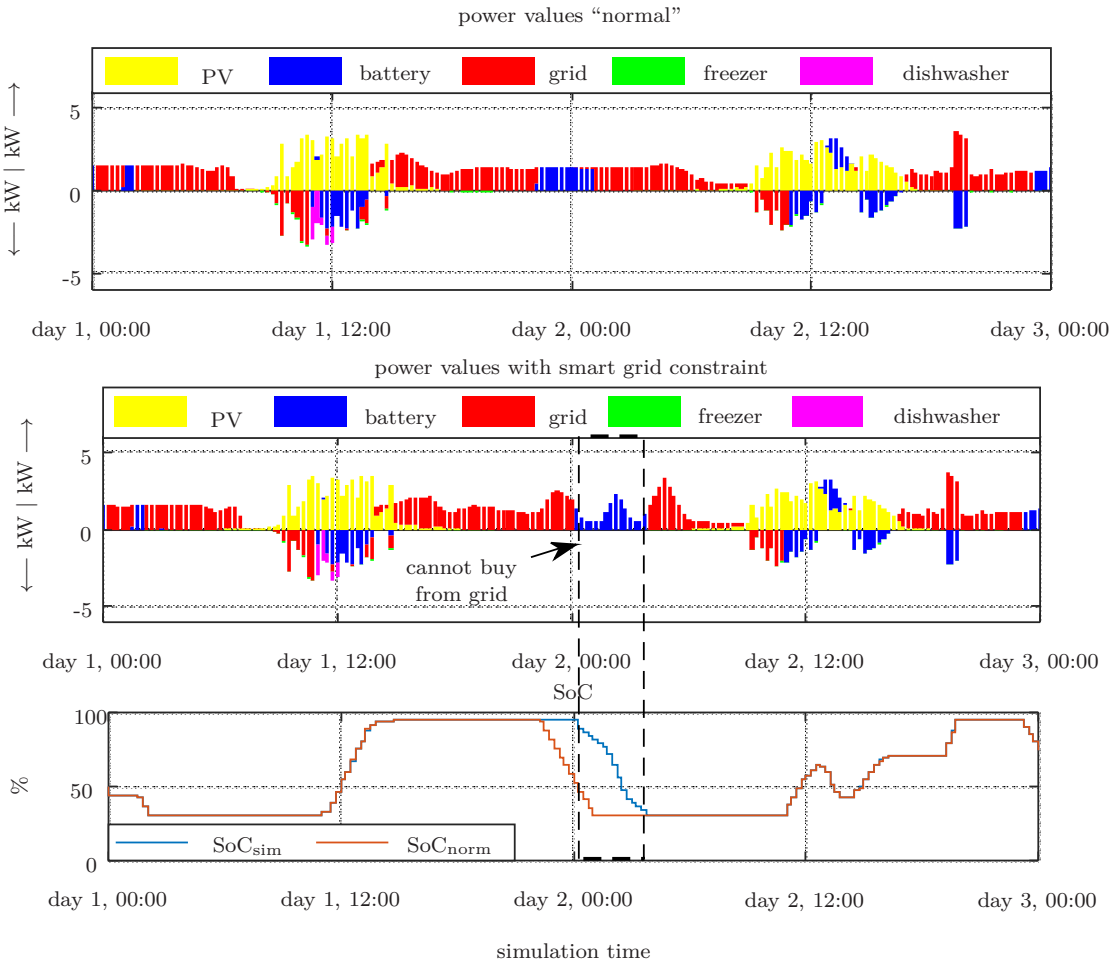

Figure 6.14: Electrical impact of grid-side load constraints. Figure from [7].

6.4 Parametric Study on MIQP-MPC Performance

The performance of model predictive control schemes depends on the available disturbance predictions. The proposed smart home controller is no exception. The performance and efficiency of the MIQP-MPC is dependent on various predictions for ambient temperature, solar irradiation, occupancy, grid prices and user generated loads. While some disturbances are known more accurate in advance, like it was assumed with the

grid prices, most of the disturbances can only be predicted. The following two subsections are showcasing how prediction quality influences the MIQP-MPC performance.

6.4.1 Weather prediction impact

To compare the impact of the proposed localized weather forecasting scheme presented in Chapter 3 a series of simulations is performed.
For a more general overview of the simulation parameters see Section 6.3. Instead of using the predictions for ambient temperature and solar irradiation provided by the weather forecasting services (WFS), the localized prediction scheme based on autoregressive models with external inputs (ARX) is applied. Another series of simulations with the real future ambient temperature and solar irradiation as predictions is carried out to serve as a benchmark. This series is denoted by the label 'real' and illustrates the best possible result for each operation mode. Note that all the simulations carried out in this subsection still utilize the occupancy prediction scheme presented in Section 4.2. The Tables 6.5-6.7 illustrate the impact of the different predictions on the earlier defined metrics and operation modes.

Table 6.5: Prediction modes comparison 'comf' mode for 7 days

Prediction mode	operating cost	grid energy	average PPD	RMSE($\vartheta_p^{\mathrm{ref}}$, $\vartheta_p^{\mathrm{act}}$)
WFS	4.54 €	123 kWh	5.12 %	0.19° C
ARX	4.53 €	123 kWh	5.13 %	0.16° C
Real	4.40 €	119 kWh	5.11 %	0.08° C

Table 6.6: Prediction modes comparison 'eco' mode for 7 days

Prediction mode	operating cost	grid energy	average PPD	RMSE($\vartheta_p^{\mathrm{ref}}$, $\vartheta_p^{\mathrm{act}}$)
WFS	3.88 €	101 kWh	5.77 %	1.05° C
ARX	3.74 €	101 kWh	5.93 %	1.21° C
Real	3.71 €	99.7 kWh	5.89 %	1.25° C

Table 6.7: Prediction modes comparison 'cost' mode for 7 days

Prediction mode	operating cost	grid energy	average PPD	RMSE($\vartheta_p^{\mathrm{ref}}$, $\vartheta_p^{\mathrm{act}}$)
WFS	3.72 €	110 kWh	5.91 %	1.24° C
ARX	3.69 €	109 kWh	5.93 %	1.28° C
Real	3.65 €	107 kWh	5.89 %	1.29° C

Note that the average PPD is non-linear and the lowest possible value is 5%. Because of the non-linearity the average PPD can actually increase slightly while the RMSE decreases. This can be seen in Table 6.5 when comparing the WFS and the ARX predictions.
By utilizing the ARX predictions instead of the WFS predictions the controller in 'eco' mode achieves 82.35 % of the possible cost savings shown by the benchmark case. When in 'cost' mode the controller accomplishes 42.86 % of the benchmark case operating cost reduction. Even in 'comf' mode the MIQP-MPC manages to reach 7.14 % of the possible operating costs reduction. With the localized predictions this mode also achieves 27 % of the indoor temperature RMSE improvements given by the benchmark case.

6.4.2 Occupcancy Prediction Impact

This subsection illustrates the impacts of the occupancy prediction method proposed in Section 4.2 on the MIQP-MPC performance. The simulation parameters remain unchanged from those defined in Section 6.3. The predictions for ambient temperature and solar irradiation are provided by the WFS. A simulation is carried out with an accurate prediction of the occupancy. This is achieved by using the actual future occupancy data as predictions for the controller. This simulation is compared to a simulation where the adaptive occupancy prediction method is used. Figure 6.15 illustrates the thermal results of both simulations. The indoor temperature denoted by $\vartheta^{\mathrm{act}}_{\mathrm{real}}$ is the result of the simulation with the accurate occupancy prediction while $\vartheta^{\mathrm{act}}_{\mathrm{pred}}$ is the result of the adaptive occupancy prediction. The soft-constraints $\vartheta^{\mathrm{act}}_{\mathrm{real,\,min\setminus max}}$ are calculated from Equations (6.2a)-(6.2b) with the real occupancy whereas the soft-constraints $\vartheta^{\mathrm{act}}_{\mathrm{pred,\,min\setminus max}}$ are calculated with the predicted occupancy.

A noticeable difference can be seen starting from day 3, 12:00 to the end of day 5. During those days the user is present in the smart home most of the time, but the occupancy prediction is struggling to predict this behavior. A typical situation for this kind of user presence could be a sick-day. For the remaining days the adaptive algorithm has successfully identified the usual leave and coming home times. The metrics for the different MPC modes can be seen in Table 6.8.

Table 6.8: Performance modes comparison with actual future occupancy data

mode	operating cost	grid energy	average PPD	RMSE($\vartheta_p^{\mathrm{ref}}$, $\vartheta_p^{\mathrm{act}}$)
comf	4.60 €	125 kWh	5.10 %	0.22° C
eco	4.10 €	110 kWh	5.14 %	0.90° C
cost	3.92 €	112 kWh	5.13 %	1.05° C

The comparison to the results of Table 6.4 are given in Table 6.9. It is obvious that

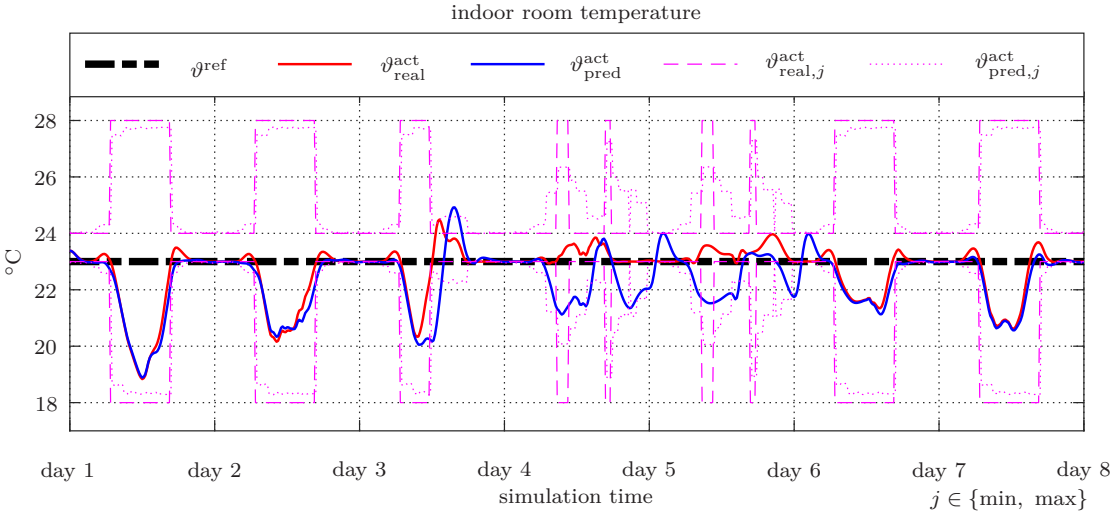

Figure 6.15: Thermal impact of occupancy prediction. For both simulations the controller was in 'cost' mode.

the average PPD was improved in all modes. Furthermore, all modes have higher operating costs and energy demands. This is because during the earlier mentioned period the smart home has to maintain a higher indoor temperature due to the certain predictions and thus requires more power. The slightly higher RMSE for the 'comf' mode is insignificant, while the lower RMSE values for the other modes showcase a much better result.

Table 6.9: Performance differences between Table 6.4 and Table 6.8

mode	operating cost	grid energy	average PPD	RMSE($\vartheta_p^{\mathrm{ref}}$, $\vartheta_p^{\mathrm{act}}$)
comf	+0.06 €	+2 kWh	−0.02 %	+0.03° C
eco	+0.22 €	+9 kWh	−0.63 %	−0.15° C
cost	+0.20 €	+2 kWh	−0.78 %	−0.19° C

Chapter 7

Discussion

A MIQP-MPC has been proposed for thermal control as well as energy management in smart homes. The defining feature of the controller formulation is that it includes both, a thermal model and the electrical model of the smart home. This allows the MIQP-MPC to solve both problem statements given by the models in one iteration and therefor globally optimize the entire smart home. One of the drawbacks of MPC scheme is that the performance is depending on the quality of the available predictions of disturbances of the prediction horizon. The proposed prediction scheme for localized weather forecasts has demonstrated that it not only improves the available weather forecasts but also reduces the operating costs of the smart home. The suggested occupancy prediction algorithm is self-learning and adaptive and therefore excellently suited for the task. Furthermore, the occupancy prediction algorithm could be further improved by separating weekdays and weekends/holidays during the feature extraction.
Another drawback of MPCs are the long computation times and the complex solving algorithms needed. Since a common sampling time of $T_s = .25$ hours was used, real time control via MPC is possible. Tuning the controller can be achieved by the end-user via the proposed method for generating the user weights as the interface is easy to use and intuitive. Especially older generations and people who do not use thermostats that often should benefit from the simplicity of the concept.

The research questions asked in Section 1.3 are being answered below:

Is it possible to improve the general weather forecast by using measurements taken from a weather station to form a localized prediction?
An ARX-model based localized weather forecasting scheme for ambient temperature as well as solar irradiation has been proposed for smart homes. With the aid of this scheme the ambient temperature can be predicted more accurately over the whole prediction horizon. The short term predictions up to 3 hours are vastly improved and

the long term predictions also offer an improvement compared to regular WFS. The solar irradiation forecasting scheme offers a method to account for changing weather conditions overnight. This allows the ARX-model to tune the parameters for the new conditions without relying on measurements. The short term improvements offer more accurate results. For the performance numbers of the improved forecasts, see the last paragraph. The solar predictions can only be calculated till sundown, reducing the sample size for the long term predictions. The smaller sample size also increases the uncertainties when interpreting the results. Although the numeric results indicate an improved RMSE for the long term irradiation predictions, further data should be collected and investigated. Weather stations are already standard equipment in modern smart homes. Those weather stations usually collect ambient temperature and solar irradiation along with humidity. Furthermore, the smart home controllers are usually able to connect to the Internet and send/receive data, allowing them to retrieve predictions form WFS. This would enable modern smart homes to implement the presented localized weather forecasting scheme with little to no additional costs for the end-user.

What are the formulations and benefits of a combined controller for building temperature control and electrical system management?
The presented MIQP-MPC controller offers various benefits compared to conventional controllers used in smart homes. The MIQP-MPC guarantees the thermal comfort in the smart home while also optimizing the monetary costs and smart grid consumed energy. Due to the combination of the QP problem given by the thermal smart home model and the MILP problem given by the electrical smart home model the MIQP-MPC is able to do the comfort management as well as the electrical management. This enables the MIQP-MPC to optimally shift electrical loads, including heating, to minimize costs or account for possible energy shortages. The combined controller is well suited for demand side load constraints imposed on the smart home by smart grids as demonstrated by the results. Furthermore, smart appliances have been implemented to showcase the flexibility of the controller when scheduling loads. The thermal model also enables the smart home to utilize the thermal capacity of the building. This enables the usage of smaller residential battery systems. The performance results are given by given closed-loop simulations and showcase the advantages and effectiveness of the MIQP-MPC for the mentioned cases.

How does a model predictive controller for a smart home benefit from improved weather forecasts or occupancy predictions?
The introduced localized weather forecasting method for generating improved ambient temperature predictions and solar irradiation predictions offer significant advantages in reducing the operating costs. In one example the localized weather forecast managed

to achieve 82.35 % of the potential savings compared to traditional WFS. While the more accurate predictions did not obtain a significant reduction of consumed energy, they did reduce the temperature RMSE in the 'cost' mode significantly. The occupancy prediction method proposed in Section 4.2 is based on extracting statistical features of smart home based sensors. The extracted features represent usual daily occupancy trajectories. While the algorithm is self-learning and switches reliable between identified occupancy trajectories, it is still limited by being solely based on sensors inside the smart home. Thus, it can only react to unpredicted occupancy once the user enters the smart home. A more sophisticated occupancy prediction method will improve the user comfort, but it is questionable if further cost and energy savings can be achieved. In the investigated cases the resident had a fairly regular schedule during most days which was learned by the prediction algorithm and predicted accurately. During those days the smart home controller was able to utilize the times without occupancy for energy and cost saving purposes.

Bibliography

[1] EAE European Association for external thermal insulation composite systems. Energy saving guide 2016. `https://www.ea-etics.eu`. Accessed: 2018-01-04.

[2] EU European Union. Directive 2010/31/eu of the european parliament and of the council of 19 may 2010 on the energy performance of buildings (recast), 6 2010.

[3] Haider Tarish Haider, Ong Hang See, and Wilfried Elmenreich. A review of residential demand response of smart grid. *Renewable and Sustainable Energy Reviews*, 59:166–178, 2016.

[4] Gaudenz Koeppel and Magnus Korpas. Using storage devices for compensating uncertainties caused by non-dispatchable generators. In *Probabilistic Methods Applied to Power Systems, 2006. PMAPS 2006. International Conference on*, pages 1–8. IEEE, 2006.

[5] Ge Gao and Kamin Whitehouse. The self-programming thermostat: optimizing setback schedules based on home occupancy patterns. In *Proceedings of the First ACM Workshop on Embedded Sensing Systems for Energy-Efficiency in Buildings*, pages 67–72. ACM, 2009.

[6] Antimo Barbato, Antonio Capone, Giuliana Carello, Maurizio Delfanti, Davide Falabretti, and Marco Merlo. A framework for home energy management and its experimental validation. *Energy Efficiency*, 7(6):1013–1052, 2014.

[7] M. Killian, M. Zauner, and M. Kozek. Smart home energy management system with smart appliances using mixed-integer quadratic-programming. *Applied Energy*, 2018. ISSN: 0306-2619, under review.

[8] Samuel Prívara, Ji***r***í Cigler, Zden***e***k Vá***n***a, Frauke Oldewurtel, Carina Sagerschnig, and Eva ***Z***á***c***eková. Building modeling as a crucial part for building predictive control. *Energy and Buildings*, 56:8 – 22, 2013.

[9] Samuel F. Fux, Araz Ashouri, Michael J. Benz, and Lino Guzzella. Ekf based self-adaptive thermal model for a passive house. *Energy and Buildings*, 68:811 – 817, 2014.

[10] C.P. Underwood. An improved lumped parameter method for building thermal modelling. *Energy and Buildings*, 79:191 – 201, 2014.

[11] M. Killian, B. Mayer, and M. Kozek. Effective fuzzy black-box modeling for building heating dynamics. *Energy and Buildings*, 96:175 – 186, 2015.

[12] Francesco Ferracuti, Alessandro Fonti, Lucio Ciabattoni, Stefano Pizzuti, Alessia Arteconi, Lieve Helsen, and Gabriele Comodi. Data-driven models for short-term thermal behaviour prediction in real buildings. *Applied Energy*, 204:1375 – 1387, 2017.

[13] Elisabeth Luchini, Alexander Schirrer, and Martin Kozek. A hierarchical mpc for multi-objective mixed-integer optimisation applied to redundant refrigeration circuits. *IFAC-PapersOnLine*, 50(1):9058 – 9064, 2017. 20th IFAC World Congress.

[14] Joshua S Stein. The photovoltaic performance modeling collaborative (pvpmc). In *Photovoltaic Specialists Conference (PVSC), 2012 38th IEEE*, pages 003048–003052. IEEE, 2012.

[15] Peder Bacher, Henrik Madsen, and Henrik Aalborg Nielsen. Online short-term solar power forecasting. *Solar Energy*, 83(10):1772–1783, 2009.

[16] Leen Peeters, Richard De Dear, Jan Hensen, and William D'haeseleer. Thermal comfort in residential buildings: Comfort values and scales for building energy simulation. *Applied Energy*, 86(5):772–780, 2009.

[17] Poul O Fanger et al. Thermal comfort. analysis and applications in environmental engineering. *Thermal comfort. Analysis and applications in environmental engineering.*, 1970.

[18] S Karjalainen. Thermal comfort and gender: a literature review. *Indoor air*, 22(2):96–109, 2012.

[19] Sami Karjalainen. Gender differences in thermal comfort and use of thermostats in everyday thermal environments. *Building and environment*, 42(4):1594–1603, 2007.

[20] Ken C Parsons. The effects of gender, acclimation state, the opportunity to adjust clothing and physical disability on requirements for thermal comfort. *Energy and Buildings*, 34(6):593–599, 2002.

[21] Nobuko Hashiguchi, Yue Feng, and Yutaka Tochihara. Gender differences in thermal comfort and mental performance at different vertical air temperatures. *European journal of applied physiology*, 109(1):41–48, 2010.

[22] J van Hoof, L Schellen, V Soebarto, JKW Wong, and JK Kazak. Ten questions concerning thermal comfort and ageing. *Building and Environment*, 120:123–133, 2017.

[23] ISO. Ergonomics of the thermal environment – analytical determination and interpretation of thermal comfort using calculation of the pmv and ppd indices and local thermal comfort criteria, (2005). *ISO, International standard 7730*.

[24] Rasmus Halvgaard, Niels Kjølstad Poulsen, Henrik Madsen, and John Bagterp Jørgensen. Economic model predictive control for building climate control in a smart grid. In *Innovative Smart Grid Technologies (ISGT), 2012 IEEE PES*, pages 1–6. IEEE, 2012.

[25] M.Killian and M. Kozek. Adaptive modeling and short-term occupancy prediction for model predictive control of smart homes. In *Proceedings of the 17th European Control Conference (ecc18)*. June 12-15, 2018, Limassol, Cyprus, submitted.

[26] YC Liang, HP Lee, SP Lim, WZ Lin, KH Lee, and CG Wu. Proper orthogonal decomposition and its applications—part i: Theory. *Journal of Sound and vibration*, 252(3):527–544, 2002.

[27] Rakesh Agrawal, Johannes Gehrke, Dimitrios Gunopulos, and Prabhakar Raghavan. *Automatic subspace clustering of high dimensional data for data mining applications*, volume 27. ACM, 1998.

[28] Eugene L Lawler and David E Wood. Branch-and-bound methods: A survey. *Operations research*, 14(4):699–719, 1966.

[29] Manfred Padberg and Giovanni Rinaldi. A branch-and-cut algorithm for the resolution of large-scale symmetric traveling salesman problems. *SIAM review*, 33(1):60–100, 1991.

[30] Hugues Marchand, Alexander Martin, Robert Weismantel, and Laurence Wolsey. Cutting planes in integer and mixed integer programming. *Discrete Applied Mathematics*, 123(1):397–446, 2002.

[31] Gurobi GmbH. Gurobi optimizer. `http://www.gurobi.com`. Accessed: 2018-01-18.

[32] International Standard. Iec 60904-3:2016,photovoltaic devices - part 3: Measurement principles for terrestrial photovoltaic (pv) solar devices with reference spectral irradiance data.

[33] Sebastian Gottwalt, Wolfgang Ketter, Carsten Block, John Collins, and Christof Weinhardt. Demand side management—a simulation of household behavior under variable prices. *Energy policy*, 39(12):8163–8174, 2011.